axoplasmic NA accumulation and reduction of the Na^+ gradient cause reverse transport of NA from the intracellular space to the extracellular space (Schwartz 2000). Acute myocardial ischaemia evokes the myocardial interstitial NA release in the ischaemic region via retrograde NA transport, independently of efferent sympathetic nerve activity (Schömig *et al.* 1984, Yamazaki *et al.* 1996, Akiyama & Yamazaki 1999, Kawada *et al.* 2001a).

Similar to NA, choline and glutamate are taken up into cells by plasma membrane transporters driven by the Na^+ gradient (Schwartz 2000). We hypothesized that the loss of Na^+ gradient under ischaemic conditions would interfere with the transporter function, which would in turn alter myocardial interstitial choline and glutamate levels. Choline release has been suggested as an index of ischaemic degradation of the myocardial phospholipid bilayer in isolated, Tyrode solution-perfused rat hearts (Brühl *et al.* 2004). Glutamate can be a preferred myocardial fuel during ischaemia and may have protective effects on ischaemic myocardium (Arsenian 1998). Measuring myocardial interstitial levels of these molecules *in vivo* would contribute to understanding the pathophysiology of acute myocardial ischaemia. To test the hypothesis, we employed an *in vivo* cardiac microdialysis technique and measured myocardial interstitial choline and glutamate levels in anaesthetized cats (Akiyama *et al.* 1991, 1994, Yamazaki *et al.* 1997, Kawada *et al.* 2001b). Acute myocardial ischaemia inevitably affects systemic haemodynamics and perfusion of the heart. To minimize such haemodynamic effects, we also examined the effects of Na^+,K^+-ATPase inhibition on the myocardial interstitial choline and glutamate levels by locally administering ouabain through a dialysis probe (Yamazaki *et al.* 1999, Kawada *et al.* 2002). The results of the present study indicated that the myocardial interstitial choline level was not increased by acute myocardial ischaemia or by Na^+,K^+-ATPase inhibition. By contrast, the myocardial interstitial glutamate level was increased by both interventions. The glutamate transporter contributed to glutamate release via retrograde transport.

Materials and methods

Surgical preparation

Animal care was conducted in strict accordance with the *Guiding Principles for the Care and Use of Animals in the Field of Physiological Sciences* approved by the Physiological Society of Japan. Adult cats weighing 2.0–4.8 kg were anaesthetized via an intraperitoneal injection of pentobarbital sodium (30–35 mg kg^{-1}) and ventilated mechanically with room air mixed with oxygen. The depth of anaesthesia was maintained with a continuous intravenous infusion of pentobarbital sodium (1–2 mg kg^{-1} h^{-1}) through a catheter inserted via the right femoral vein. Mean systemic arterial pressure was monitored from a catheter inserted via the right femoral artery.

With the animal in the lateral position, the left fifth and sixth ribs were resected to expose the heart. When a coronary occlusion was necessary, a 3-0 silk suture was prepared around the left anterior descending coronary artery (LAD) just distal to the first diagonal branch. With a fine guiding needle, a dialysis probe was implanted into the left ventricular free wall perfused by the LAD. Heparin sodium (100 U kg^{-1} bolus injection followed by a maintenance dose of 50 U kg^{-1} h^{-1}) was administered intravenously to prevent blood coagulation. At the end of the experiment the experimental animals were killed by an overdose of pentobarbital sodium. We confirmed that the dialysis probe had been implanted within the left ventricular myocardium.

Dialysis technique

We designed a transverse dialysis probe (Akiyama *et al.* 1991, 1994). For measurements of small molecular compounds including ACh, choline, and glutamate, we used a dialysis fibre of 50 000 molecular weight cutoff (13 mm length, 310 μm OD, 200 μm ID; PAN-1200, Asahi Chemical, Osaka, Japan) with both ends glued to polyethylene tubes (20 cm length, 500 μm OD, 200 μm ID). The dialysis probe was perfused at a rate of 2 μL min^{-1} with Ringer solution. Each sample was collected in a microtube containing 3 μL of phosphate buffer (100 mM, pH 3.5). A cholinesterase inhibitor eserine (100 μM) was added to the perfusate to measure ACh. A preliminary examination indicated that whether the perfusate-contained eserine did not affect myocardial interstitial choline levels significantly. Dead space volume between the dialysis fibre and the sample microtube was identical for ACh, choline, and glutamate measurements, and the sampling was performed taking into account the time for dialysate to traverse the dead space volume.

The dialysate ACh and choline levels were measured directly by high-performance liquid chromatography with electrochemical detection. The absolute detection limits of ACh and choline, determined with a signal-to-noise ratio of 3, were 10 and 5 fmol per injection, respectively. The dialysate glutamate level was measured by kinetic enzymatic analysis with CMA 600. The absolute detection limit of glutamate was 1 μM per injection.

Protocols

All protocols were started from 2 h after implanting the dialysis probe. To examine changes in myocardial

interstitial ACh and choline levels during acute myocardial ischaemia ($n = 6$), after collecting a 15-min baseline dialysate sample, we occluded the LAD for 60 min and obtained four consecutive 15-min dialysate samples. The full-length of the implanted dialysis fibre was located within the ischaemic area judged by discoloration of myocardium during the LAD occlusion. We then released the occlusion and collected a 15-min dialysate sample during reperfusion. To examine changes in myocardial ACh and choline levels in response to local ouabain administration ($n = 6$), after collecting a 15-min baseline dialysate sample, we replaced the perfusate with Ringer solution containing 100 μM ouabain and collected four consecutive 15-min dialysate samples.

In different groups of animals, myocardial interstitial glutamate levels were measured during acute myocardial ischaemia ($n = 6$) and during local administration of ouabain ($n = 6$). To elucidate the role of the glutamate transporter, we also examined the effects of glutamate transport inhibition by *trans*-L-pyrrolidine-2,4-dicarboxylate (*t*-PDC, 10 mM) on myocardial interstitial glutamate levels during acute myocardial ischaemia ($n = 7$) and local administration of ouabain ($n = 7$). *t*-PDC was locally administered through the dialysis probe to avoid systemic effects.

Statistical analysis

All data are presented as mean ± SE values. In each protocol, the effects of myocardial ischaemia or local ouabain administration were examined using one-way analysis of variance followed by Dunnett's test against the corresponding baseline level (Glantz 2002). The baseline as well as maximum glutamate levels with and without glutamate transport inhibition were compared by an unpaired *t*-test during acute myocardial ischaemia or during local ouabain administration (Glantz 2002). Differences were considered to be significant when $P < 0.05$.

Results

Figure 1a shows myocardial interstitial ACh level during acute myocardial ischaemia. The ACh level was increased by LAD occlusion, becoming approximately 15 times higher than the baseline level at 30–45 and 45–60 min of ischaemia. The ACh level decreased towards the baseline level upon reperfusion. Figure 1b illustrates myocardial interstitial choline level during acute myocardial ischaemia. The choline level did not change significantly throughout the ischaemic and reperfusion periods.

Figure 2a shows changes in myocardial interstitial ACh level during local administration of ouabain. The ACh level was increased by the inhibition of

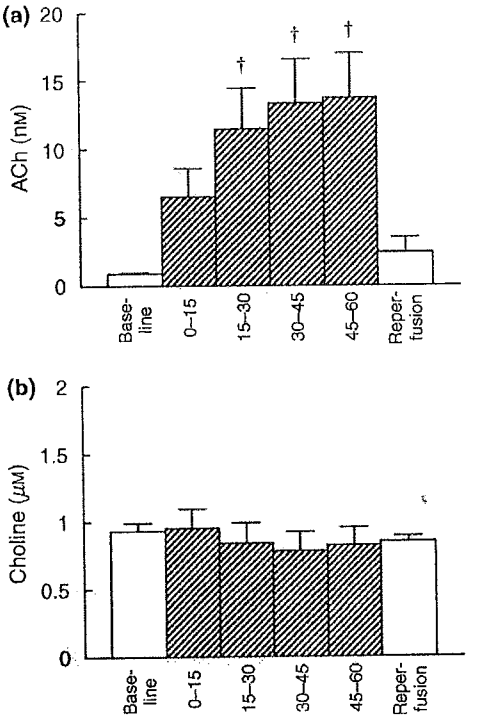

Figure 1 Changes in myocardial interstitial acetylcholine (ACh) level (a) and choline level (b) during coronary artery occlusion and reperfusion. Myocardial interstitial ACh level was significantly increased by acute myocardial ischaemia, while myocardial interstitial choline level was not changed. Data are mean ± SE. †$P < 0.01$ from baseline.

Na^+,K^+-ATPase, becoming approximately nine times higher than the baseline level at 15–30 min. The ACh level then decreased but remained significantly higher than the baseline level. Figure 2b illustrates the myocardial interstitial choline level during local administration of ouabain. The choline level was significantly lower at 0–15 and 45–60 min when compared with the baseline level.

Figure 3a shows changes in myocardial interstitial glutamate level during acute myocardial ischaemia. LAD occlusion increased the glutamate level to approximately 3.5 times higher than the baseline level at 0–15 min. Thereafter, the glutamate level was significantly higher than the baseline level throughout the ischaemic and reperfusion periods. Figure 3b illustrates the effects of glutamate transport inhibition on the ischaemia-induced glutamate release. The baseline glutamate level was significantly decreased by glutamate transport inhibition ($P < 0.05$). Although acute myocardial ischaemia and reperfusion significantly increased the glutamate level relative to the baseline level, the maximum glutamate level was attenuated to approximately one-fifth compared with that observed without glutamate transport inhibition ($P < 0.05$).

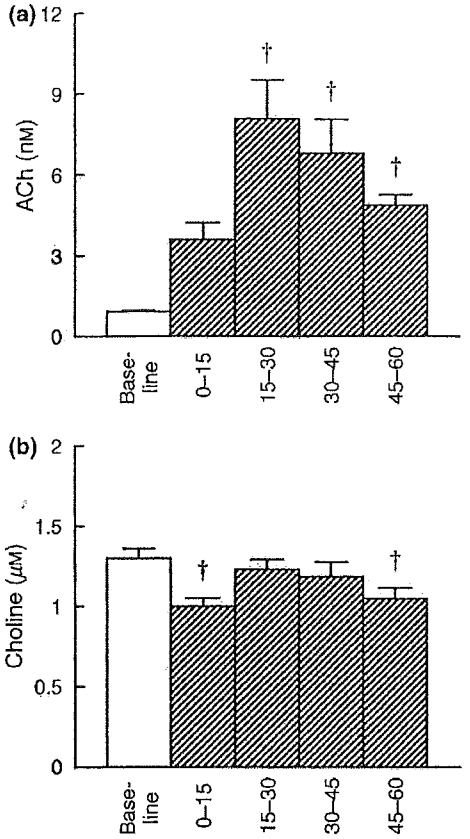

Figure 2 Changes in myocardial interstitial acetylcholine (ACh) level (a) and choline level (b) in response to the local administration of ouabain. Myocardial interstitial ACh level was significantly increased by ouabain. In contrast, myocardial interstitial choline level was decreased by ouabain. Data are mean ± SE. †$P < 0.01$ from baseline.

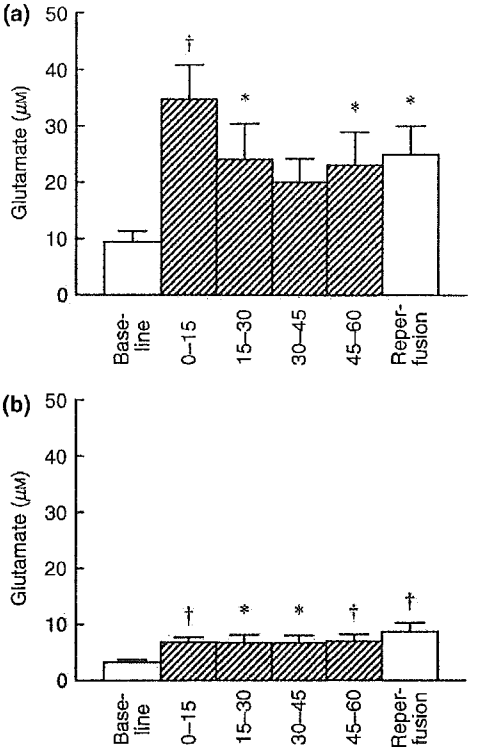

Figure 3 Changes in myocardial interstitial glutamate level during coronary artery occlusion and reperfusion without (a) and with (b) the inhibition of glutamate transporter. The glutamate level was significantly increased by acute myocardial ischaemia. The ischaemia-induced glutamate release was suppressed by the inhibition of glutamate transporter. Data are mean ± SE. †$P < 0.01$ and *$P < 0.05$ from baseline.

Figure 4a shows changes in myocardial interstitial glutamate level during the local administration of ouabain. Ouabain administration did not change the glutamate level at 0–15 min but increased the glutamate level thereafter. The glutamate level became approximately 1.8 times higher than the baseline level at 30–45 min. Figure 4b illustrates the effects of glutamate transport inhibition on ouabain-induced glutamate release. The baseline glutamate level was significantly decreased by the inhibition of glutamate transport ($P < 0.05$). Although ouabain administration increased the glutamate level relative to the baseline level, the maximum glutamate level was suppressed to approximately one-third of that observed without glutamate transport inhibition ($P < 0.05$).

Discussion

We have shown that acute myocardial ischaemia and local inhibition of Na^+,K^+-ATPase increased myocardial interstitial glutamate level but not choline level. Despite the similar Na^+ gradient dependency of corresponding transporters, myocardial interstitial glutamate and choline levels showed differential responses to the two interventions.

Changes in myocardial interstitial choline level

In the vagal nerve endings, ACh is hydrolysed to acetate and choline by acetylcholinesterase (Nicholls 1994). Choline is then taken up into the vagal nerve endings by the choline transporter driven by the Na^+ gradient. We hypothesized that loss of Na^+ gradient during acute myocardial ischaemia or local ouabain administration would increase the myocardial interstitial choline level by the interruption of choline uptake. Contrary to our hypothesis, acute myocardial ischaemia did not change myocardial interstitial choline level in the ischaemic region (Fig. 1b). Ouabain administration decreased the myocardial interstitial choline level at 0–15 and 45–60 min (Fig. 2b).

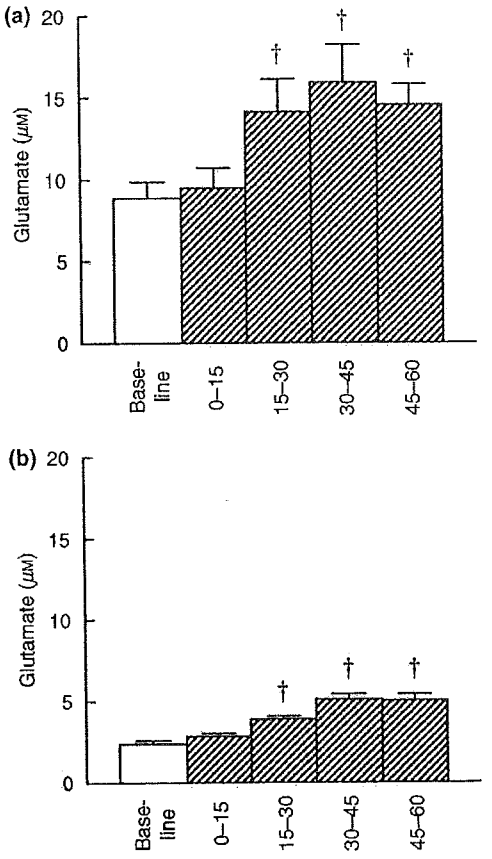

Figure 4 Changes in myocardial interstitial glutamate level in response to the local administration of ouabain without (a) and with (b) the inhibition of glutamate transporter. The glutamate level was significantly increased by ouabain administration. The ouabain-induced glutamate release was suppressed by the inhibition of glutamate transporter. Data are mean ± SE. †$P < 0.01$ from baseline.

Possible explanations for the absence of ischaemia- or ouabain-induced choline release are as follows. First, choline uptake is the rate-limiting step for ACh synthesis (Lockman & Allen 2002). Because choline in the intracellular space is rapidly consumed for ACh synthesis, the axoplasmic choline concentration might have been too low to evoke reverse transport by the choline transporter. Second, plasma choline concentration is stabilized by *de novo* choline synthesis from the catabolism of phosphatidylcholine found in cell membranes (Lockman & Allen 2002). Potential choline release may have been counterbalanced by the local stabilization mechanisms. Taking into account the recovery rate of the dialysis probe (approximately 30%), the myocardial interstitial choline concentration was 3–5 μM. Although the estimated concentration was lower than the highly regulated plasma choline concentration of approximately 10 μM, it was much higher than the ischaemia-induced maximum choline release (approximately 0.6 μM) in isolated rat hearts reported by Brühl *et al.* (2004). The present results suggest that myocardial interstitial choline level may not serve as an indicator of myocardial ischaemia in blood-perfused *in vivo* feline hearts.

By contrast with myocardial interstitial choline level, myocardial interstitial ACh level was increased both by acute myocardial ischaemia and by local administration of ouabain. Because ischaemia-induced ACh release was observed after vagal nerve transection in a previous study (Kawada *et al.* 2000), a Ca^{2+} channel-independent, regional release mechanism appears to be involved. Several reports have suggested that ouabain or ischaemia-induced intracellular Na^+ accumulation could elevate intracellular Ca^{2+} level via Na^+/Ca^{2+} exchange (Mochizuki & Jiang 1998, Li *et al.* 2000). The elevation of intracellular Ca^{2+} level may be associated with ACh release. Our previous study indicated that intracellular Ca^{2+} overload due to Ca^{2+} mobilization is responsible for the ACh release evoked by ischaemia (Kawada *et al.* 2000).

Changes in myocardial interstitial glutamate levels

Although the glutamate transporter family differs from the NA transporter family in that it requires countertransport of K^+ instead of cotransport of Cl^-, its primary driving force is the Na^+ gradient across the plasma membrane (Schwartz 2000). Therefore, interventions that reduce the Na^+ gradient are likely to cause reverse transport of glutamate, in a similar manner to the reverse transport of NA. Acute myocardial ischaemia increased the myocardial interstitial glutamate level (Fig. 3a) as consistent with previous reports (Kennergren *et al.* 1997, 1999, Bäckström *et al.* 2003, Song *et al.* 1996). Inhibition of Na^+,K^+-ATPase also induced myocardial interstitial glutamate release (Fig. 4a). Glutamate release during acute myocardial ischaemia and local ouabain administration was significantly attenuated by the inhibition of glutamate transport (Figs 3b and 4b), suggesting the involvement of reverse transport by the glutamate transporter. Glutamate plays a vital role in keeping nitrogen balance in cells as a common amino acid in transamination reactions. The high intra-to-extracellular concentration ratio of glutamate would contribute to the retrograde transport by the glutamate transporter during the loss of normal Na^+ gradient.

In the case of myocardial interstitial NA levels, local blockade of NA uptake increased baseline NA levels, suggesting the accumulation of NA spontaneously released into the synaptic cleft (Akiyama & Yamazaki 1999). We therefore predicted that the inhibition of glutamate transport would increase the baseline gluta-

mate level. However, the inhibition of glutamate transport actually decreased the baseline glutamate level (Figs 3 and 4), suggesting that spontaneous glutamate release rather than glutamate uptake had occurred under baseline conditions. The insertion of a dialysis probe inevitably damages the myocardium. Although we waited for 2 h after implantation of the dialysis probe and the glutamate level declined with time, glutamate release from damaged myocardium may have continued. Notwithstanding this limitation, we were able to detect glutamate release in response to acute myocardial ischaemia and inhibition of Na^+,K^+-ATPase. Therefore, our interpretation that glutamate release was dependent on the reverse transport of glutamate transporter may be reasonable.

Supplementing the heart with glutamate has been shown to have beneficial effect on the recovery of contractile function in post-surgical patients (Arsenian 1998). The myocardial interstitial glutamate level remained increased during 15-min reperfusion whereas the myocardial interstitial ACh level returned towards the baseline level. Although the reason for different responses upon reperfusion was unanswered in the present study, the sustained increase in the glutamate level may have therapeutic effect on its own.

In conclusion, acute myocardial ischaemia and inhibition of Na^+,K^+-ATPase did not increase myocardial interstitial choline level despite a significant increase in myocardial interstitial ACh level. By contrast, both interventions significantly increased the myocardial interstitial glutamate level. The glutamate transporter contributed to myocardial interstitial glutamate release via retrograde transport.

This study was supported by Health and Labour Sciences Research Grant for Research on Advanced Medical Technology (H14-Nano-002) from the Ministry of Health Labour and Welfare of Japan, by Grant-in-Aid for Scientific Research (C-15590786) from the Ministry of Education, Science, Sports and Culture of Japan, and by the Program for Promotion of Fundamental Studies in Health Science of the Organization for Pharmaceutical Safety and Research from Pharmaceuticals and Medical Devices Agency (PMDA).

References

Akiyama, T. & Yamazaki, T. 1999. Norepinephrine release from cardiac sympathetic nerve endings in the in vivo ischemic region. *J Cardiovasc Pharmacol* 34(Suppl. 4), S11–S14.

Akiyama, T., Yamazaki, T. & Ninomiya, I. 1991. In vivo monitoring of myocardial interstitial norepinephrine by dialysis technique. *Am J Physiol Heart Circ Physiol* 261, H1643–H1647.

Akiyama, T., Yamazaki, T. & Ninomiya, I. 1994. In vivo detection of endogenous acetylcholine release in cat ventricles. *Am J Physiol Heart Circ Physiol* 266, H854–H860.

Arsenian, M. 1998. Potential cardiovascular applications of glutamate, aspartate, and other amino acids. *Clin Cardiol* 21, 620–624.

Bäckström, T., Goiny, M., Lockowandt, U., Liska, J. & Franco-Cereceda, A. 2003. Cardiac outflow of amino acids and purines during myocardial ischemia and reperfusion. *J Appl Physiol* 94, 1122–1128.

Brühl, A., Hafner, G. & Löffelholz, K. 2004. Release of choline in the isolated heart, an indicator of ischemic phospholipid degradation and its protection by ischemic preconditioning: no evidence for a role of phospholipase D. *Life Sci* 75, 1609–1620.

Glantz, S.A. 2002. *Primer of Biostatistics*, 5th edn. McGraw-Hill, New York.

Hearse, D.J. 1979. Oxygen deprivation and early myocardial contractile failure: a reassessment of the possible role of adenosine triphosphate. *Am J Cardiol* 44, 1115–1121.

Kawada, T., Yamazaki, T., Akiyama, T. *et al.* 2000. Differential acetylcholine release mechanisms in the ischemic and non-ischemic myocardium. *J Mol Cell Cardiol* 32, 405–414.

Kawada, T., Yamazaki, T., Akiyama, T. *et al.* 2001a. Vagosympathetic interactions in ischemia-induced myocardial norepinephrine and acetylcholine release. *Am J Physiol Heart Circ Physiol* 280, H216–H221.

Kawada, T., Yamazaki, T., Akiyama, T. *et al.* 2001b. In vivo assessment of acetylcholine-releasing function at cardiac vagal nerve terminals. *Am J Physiol Heart Circ Physiol* 281, H139–H145.

Kawada, T., Yamazaki, T., Akiyama, T. *et al.* 2002. Disruption of vagal efferent axon and nerve terminal function in the postischemic myocardium. *Am J Physiol Heart Circ Physiol* 283, H2687–H2691.

Kennergren, C., Nyström, B., Nyström, U. *et al.* 1997. In situ detection of myocardial infarction in pig by measurements of aspartate aminotransferase (ASAT) activity in the interstitial fluid. *Scand Cardiovasc J* 31, 343–349.

Kennergren, C., Mantovani, V., Lönnroth, P., Nyström, B., Berglin, E. & Hamberger, A. 1999. Extracellular amino acids as markers of myocardial ischemia during cardioplegic heart arrest. *Cardiology* 91, 31–40.

Li, S., Jiang, Q., Stys, P.K. 2000. Important role of reverse Na^+-Ca^{2+} exchange in spinal cord white matter injury at physiological temperature. *J Neurophysiol* 84, 1116–1119.

Lockman, P.R. & Allen, D.D. 2002. The transport of choline. *Drug Dev Ind Pharm* 28, 749–771.

Mochizuki, S. & Jiang, C. 1998. Na^+/Ca^{++} exchanger and myocardial ischemia/reperfusion. *Jpn Heart J* 39, 707–714.

Nicholls, D.G. 1994. *Proteins, Transmitters and Synapses*, pp. 186–199. Blackwell Science, London.

Schömig, A., Dart, A.M., Dietz, R., Mayer, E. & Kübler, W. 1984. Release of endogenous catecholamines in the ischemic myocardium of the rat. Part A: Locally mediated release. *Circ Res* 55, 689–701.

Schömig, A., Kurz, T., Richardt, G. & Schömig, E. 1988. Neuronal sodium homeostasis and axoplasmic amine concentration determine calcium-independent noradrenaline release in normoxic and ischemic rat heart. *Circ Res* 63, 214–226.

Schwartz, J.H. 2000. Neurotransmitters. In: E.R. Kandel, J.H. Schwartz & T.M. Jessell (eds) *Principles of Neural Science*, 4th edn, pp. 280–297. McGraw-Hill, New York.

Song, D., O'Regan, M.H. & Phillis, J.W. 1996. Release of the excitotoxic amino acids, glutamate and aspartate, from the isolated ischemic/anoxic rat heart. *Neurosci Lett* 220, 1–4.

Yamazaki, T., Akiyama, T., Kitagawa, H., Takauchi, Y. & Kawada, T. 1996. Elevation of either axoplasmic norepinephrine or sodium level induced release of norepinephrine from cardiac sympathetic nerve terminals. *Brain Res* 737, 343–346.

Yamazaki, T., Akiyama, T., Kitagawa, H., Takauchi, Y., Kawada, T. & Sunagawa, K. 1997. A new, concise dialysis approach to assessment of cardiac sympathetic nerve terminal abnormalities. *Am J Physiol Heart Circ Physiol* 272, H1182–H1187.

Yamazaki, T., Akiyama, T. & Kawada, T. 1999. Effects of ouabain on in situ cardiac sympathetic nerve endings. *Neurochem Int* 35, 439–445.

Artificial Baroreflex

Clinical Application of a Bionic Baroreflex System

Fumiyasu Yamasaki, MD; Takahiro Ushida, MD; Takeshi Yokoyama, DDS; Motonori Ando, PhD; Koichi Yamashita, MD; Takayuki Sato, MD

Background—We proposed a novel therapeutic strategy against central baroreflex failure: implementation of an artificial baroreflex system to automatically regulate sympathetic vasomotor tone, ie, a bionic baroreflex system (BBS), and we tested its efficacy in a model of sudden hypotension during surgery.

Methods and Results—The BBS consisted of a computer-controlled negative-feedback circuit that sensed arterial pressure (AP) and automatically computed the frequency (STM) of a pulse train required to stimulate sympathetic nerves via an epidural catheter placed at the level of the lower thoracic spinal cord. An operation rule was subsequently designed for the BBS using a feedback correction with proportional and integral gain factors. The transfer function from STM to AP was identified by a white noise system identification method in 12 sevoflurane-anesthetized patients undergoing orthopedic surgery involving the cervical vertebrae, and the feedback correction factors were determined with a numerical simulation to enable the BBS to quickly and stably attenuate an external disturbance on AP. The performance of the designed BBS was then examined in a model of orthostatic hypotension during knee joint surgery (n=21). Without the implementation of the BBS, a sudden deflation of a thigh tourniquet resulted in a 17±3 mm Hg decrease in AP within 10 seconds and a 25±2 mm Hg decrease in AP within 50 seconds. By contrast, during real-time execution of the BBS, the decrease in AP was 9±2 mm Hg at 10 seconds and 1±2 mm Hg at 50 seconds after the deflation.

Conclusions—These results suggest the feasibility of a BBS approach for central baroreflex failure. (***Circulation.*** **2006; 113:634-639.)**

Key Words: baroreceptors ■ blood pressure ■ computers ■ electrical stimulation ■ nervous system, sympathetic

The arterial baroreflex acts to maintain cerebral perfusion by quickly attenuating the effect of an external disturbance, such as the assumption of an upright position, on arterial pressure (AP).[1–4] Therefore, functional restoration of dynamic properties of the arterial baroreflex is essential for the treatment of patients with various syndromes of baroreflex failure,[5] including Shy-Drager syndrome,[6–9] baroreceptor deafferentation,[10,11] and traumatic spinal cord injuries.[12,13] However, most commonly used interventions, including salt loading,[14,15] cardiac pacing,[16,17] and adrenergic agonists,[18,19] can neither restore nor reproduce the functioning of the native vasomotor center, and most affected patients remain bedridden.

Clinical Perspective p 639

We recently developed a framework for identifying an operational rule of the vasomotor center and a prototype of a bionic baroreflex system (BBS) in rats.[20–22] The BBS consisted of a negative-feedback system controlled by a computer (ie, the artificial vasomotor center) that sensed AP and automatically computed the frequency of a pulse train required to stimulate sympathetic efferent nerves through a pair of wire electrodes placed in the celiac ganglion. Previous experimental work demonstrated that the BBS restored native baroreflex function in rats with central baroreflex failure; however, an applicable neural interface with quick and effective controllability of AP is required for application of this technology in the clinical setting. The goal of the present study was to determine the efficacy of a novel bionic technology for the intraoperative restoration of AP in the context of central baroreflex failure and to validate this technology in a clinical model of orthostatic hypotension.

Methods

All studies were approved by the institutional review committee, and all subjects gave informed consent.

Theoretical Considerations

As previously described,[20–22] the principle of the BBS is based on a negative-feedback mechanism (Figure 1). The instantaneous AP is measured by a pressure transducer connected to a computer that functions as a controller or artificial vasomotor center. Instead of the disabled native vasomotor center, the controller automatically exe-

Received September 8, 2005; revision received October 31, 2005; accepted November 21, 2005.

From the Departments of Cardiovascular Control (F.Y., M.A., T.S.), Clinical Laboratory (F.Y.), Orthopedic Surgery (T.U.), and Anesthesiology (T.Y., K.Y.), Kochi Medical School, Nankoku, Japan.

Correspondence to Fumiyasu Yamasaki, MD, Department of Clinical Laboratory, Kochi Medical School, Nankoku 783-8505, Japan. E-mail yamasakf@med.kochi-u.ac.jp

Circulation **is available at http://www.circulationaha.org** **DOI: 10.1161/CIRCULATIONAHA.105.587915**

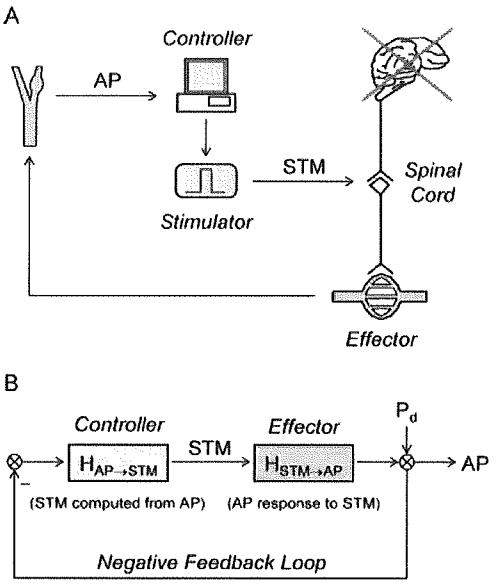

Figure 1. Schematic illustration (A) and block diagram (B) of a BBS. In the context of central baroreflex failure, the BBS automatically computes the frequency (STM) of a pulse train to stimulate sympathetic nerves through an epidural catheter placed at the level of lower thoracic spinal cord, while simultaneously sensing the change in AP. $H_{AP\rightarrow STM}$ denotes a transfer function for the controller functioning as an artificial vasomotor center. $H_{STM\rightarrow AP}$ is a transfer function showing the dynamic response of AP to STM. The overall transfer function of the BBS is given by $H_{AP\rightarrow STM}\times H_{STM\rightarrow AP}$. Therefore, the effect of an external disturbance (P_d) on AP is attenuated to $1/(1+H_{AP\rightarrow STM}\times H_{STM\rightarrow AP})$.

cutes real-time operations that determine the frequency of electrical stimulation (STM) required to minimize the effect of an external disturbance (P_d) on AP and then commands an electrical stimulator to deliver a stimulus of the same frequency to the vasomotor sympathetic nerves via epidural-catheter electrodes placed at the lower thoracic level of the spinal cord. The lower thoracic level was selected as the site for the neural interface of the BBS because the abdominal splanchnic vascular bed is a major effector mechanism for the arterial baroreflex.[23–25]

According to a classic feedback-control theory, ie, feedback correction with proportional and integral gain factors,[26,27] the following algorithm was used to program the controller for the calculation of STM in the frequency domain:

$$H_{AP\rightarrow STM}=K_p+\frac{K_i}{2\pi fj} \quad (1)$$

where $H_{AP\rightarrow STM}$ is a transfer function from AP to STM, K_p is the proportional correction factor, K_i is the integral correction factor, and j is the imaginary unit. The proportional factor determines the feedback amplification based on the absolute value of the instantaneous control error due to P_d, and the integral factor adjusts the feedback amplification based on the cumulative value of the instantaneous control error. Therefore, STM is computed as follows:

$$STM=-AP\cdot H_{AP\rightarrow STM} \quad (2)$$

and AP is also expressed as follows:

$$AP=STM\cdot H_{STM\rightarrow AP}+P_d \quad (3)$$

where $H_{STM\rightarrow AP}$ denotes the frequency response of AP to STM. From Equations 2 and 3, the effect of P_d on AP is estimated as follows:

$$AP=\frac{1}{1+H_{AP\rightarrow STM}\cdot H_{STM\rightarrow AP}}P_d \quad (4)$$

Thus, if $H_{AP\rightarrow STM}\cdot H_{STM\rightarrow AP}$ is far larger than unity, the BBS can nullify the effect of P_d on AP.

Subjects and Experimental Protocols

A total of 33 patients (46 to 84 years old, 19 males) who underwent orthopedic operations were enrolled in the present study. Ten patients had hypertension, and 4 had diabetes mellitus. None of the subjects had frequent ectopic beats or atrial fibrillation. After induction anesthesia with propofol, an endotracheal tube was introduced orally. The patients were mechanically ventilated with 67% nitrous oxide and 1.5% to 2% end-tidal sevoflurane in oxygen during experimental protocols, while end-tidal carbon dioxide was maintained at 35 to 38 mm Hg. An arterial catheter was placed in the radial artery for AP measurement. To record central venous pressure (CVP), a central venous catheter was placed in the femoral vein, and the tip of the catheter was advanced into the inferior vena cava just above the diaphragmatic level. Furthermore, an epidural catheter was placed percutaneously, and the tip, which contained a pair of electrodes (Unique Medical, Tokyo; interelectrode distance 15 mm), was placed at the level of Th_{9-11}. Placement of the central venous catheter and the epidural catheter was verified by chest radiograph.[28]

Before making an incision of affected areas, we performed 2 different protocols in separate groups of patients. In the first group of patients (n=12, 46 to 76 years old, 7 males) undergoing operations for cervical spondylosis and canal stenosis, the averaged $H_{STM\rightarrow AP}$ was estimated and the $H_{AP\rightarrow STM}$ was designed parametrically with Equation 1 to minimize the effect of P_d on AP. After we programmed the designed $H_{AP\rightarrow STM}$ into the computer, the efficacy of the BBS was tested against the rapid progressive hypotension induced by use of a thigh tourniquet[29–31] in the second group of patients (n=21, 64 to 84 years old, 12 males) undergoing operation for knee joint osteoarthritis. During each protocol, the muscle twitches induced by spinal cord stimulation were prevented by the intravenous administration of vecuronium bromide. Analgesia for the pain provoked by spinal cord stimulation and tourniquet inflation was provided by intravenous injection of fentanyl citrate. In a preliminary study, the validity of the analgesic preparation was confirmed for the experimental protocols, and the safety of spinal cord stimulation for 20 minutes was verified.

Estimation of Transfer Function From STM to AP

To characterize the dynamic nature of the AP response to STM, ie, $H_{STM\rightarrow AP}$, the lower thoracic sympathetic nerves were randomly stimulated for 15 minutes while we recorded AP. According to a white noise method for system identification, the STM was altered between 0 and 20 Hz every 4 seconds. The pulse width of electrical stimuli was fixed at 0.1 ms. The stimulation current was adjusted for each patient so as to produce a pressor response of ≈10 mm Hg at 20 Hz. This resulted in an average current of 15±4 (mean±SD) mA. The electrical signals of STM and AP were digitized at 100 Hz. As described previously,[20–22] the transfer function from STM to AP, $H_{STM\rightarrow AP}$, was estimated with a fast Fourier transform algorithm. Finally, the average of $H_{STM\rightarrow AP}$ among 12 patients was calculated.

Design of Artificial Vasomotor Center

With substitution of the averaged $H_{STM\rightarrow AP}$ for Equation 4, the instantaneous AP response to P_d was simulated numerically, and a stepwise decline with an amplitude of 20 mm Hg was imposed on the BBS. While the feedback parameters of $H_{AP\rightarrow STM}$, ie, K_p and K_i, were altered, the effect of the parameters on the AP response was investigated. Finally, the parameters that enabled the BBS to quickly and stably minimize the effect of P_d on AP were determined.

Efficacy of BBS in a Clinical Model of Transient Hypotension

The performance of the BBS was evaluated in a clinical model of rapid transient hypotension (n=21). Rapid hypotension was evoked by the sudden deflation of a thigh tourniquet, which is widely used to achieve bloodless dissection during total knee arthroplasty.[29–31] Acute hypotension immediately after tourniquet release is a well-

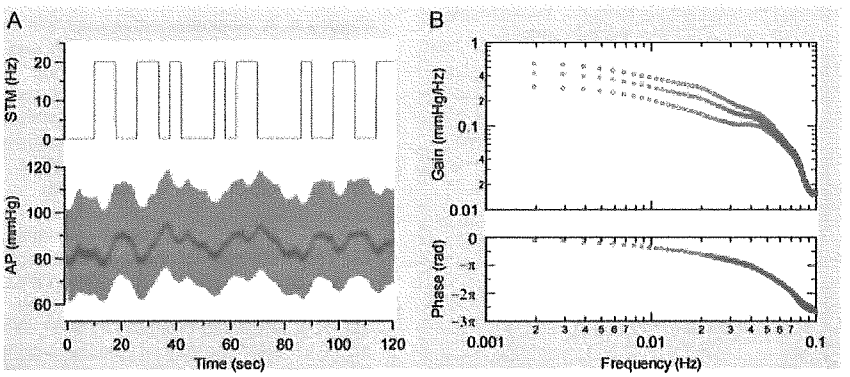

Figure 2. A, Representative example of time series data of the response of AP to random stimulation of the lower thoracic spinal cord. According to quasi-white noise, the STM was randomly altered between 0 and 20 Hz. The AP seems to slowly respond to STM with a delay. B, Transfer function of the AP response to the STM change. Data are expressed as mean±SD for 12 patients. rad indicates radians. See text for explanation.

known phenomenon that results from a rapid decrease in peripheral vascular resistance and an increase in venous pooling in the affected limb.[29] The degree of hypotension can be potentiated by the use of volatile anesthetic agents such as sevoflurane, which are central depressants of arterial baroreflex function.[32,33] Therefore, tourniquet-related hypotension during sevoflurane anesthesia can be used as a model of orthostatic hypotension in central baroreflex failure.

Briefly, a tourniquet was applied to the upper femur and inflated at 300 mm Hg for 60 minutes and then quickly deflated for 10 minutes. The procedure was then repeated. The BBS was activated during 1 of the 2 trials of tourniquet-related hypotension, and the electrical signals of STM, CVP, and AP were digitized at 100 Hz.

Statistical Analysis

The hemodynamic responses to tourniquet release were measured for each subject while the BBS was being activated and inactivated. The effects of the BBS execution on the hemodynamic changes at 10, 50, and 100 seconds after tourniquet release were analyzed by paired *t* tests with Bonferroni adjustment. Differences were considered significant at overall $P<0.05$.

Results

A representative example of original tracings of STM and AP during random stimulation of the spinal cord is shown in Figure 2A. Random on-off change in STM produced a delayed and slow change in AP. The relationship between STM and AP was quantitatively characterized by the frequency domain analysis (Figure 2B). The averaged transfer function from STM to AP, $H_{STM \rightarrow AP}$, had low-pass characteristics with a corner frequency of 0.06 Hz. The gain factor was 0.43 ± 0.13 mm Hg · Hz^{-1} at the steady state (lowest frequency) and gradually decreased with input frequency. The phase spectrum showed that the input-output relationship was in phase and that the phase delay increased toward higher frequencies. The squared coherence, a measure of linear dependence between STM and AP, was >0.9 in the frequency range of interest (data not shown).

The results of simulation for the design of the artificial vasomotor center, $H_{AP \rightarrow STM}$, are presented in Figure 3. The AP responses to the external disturbance P_d were simulated under 12 different combinations with feedback correction factors. Without feedback compensation, ie, when both feedback correction factors were zero, there was no attenuation of the effect of the external disturbance on AP. Therefore, AP fell by 20 mm Hg immediately after the imposition of P_d (Figure 3A, black line). By contrast, if either or both of the correction factors were too large, the underdamped oscillatory response of AP appeared, and the BBS became unstable. On the basis of these results, K_p was set at 1, and K_i was set at 0.1, so that the BBS could quickly and effectively attenuate the effect of the external disturbance (Figure 3B, red line).

A representative example of the results of the performance tests of the BBS is shown in Figure 4A. A sudden

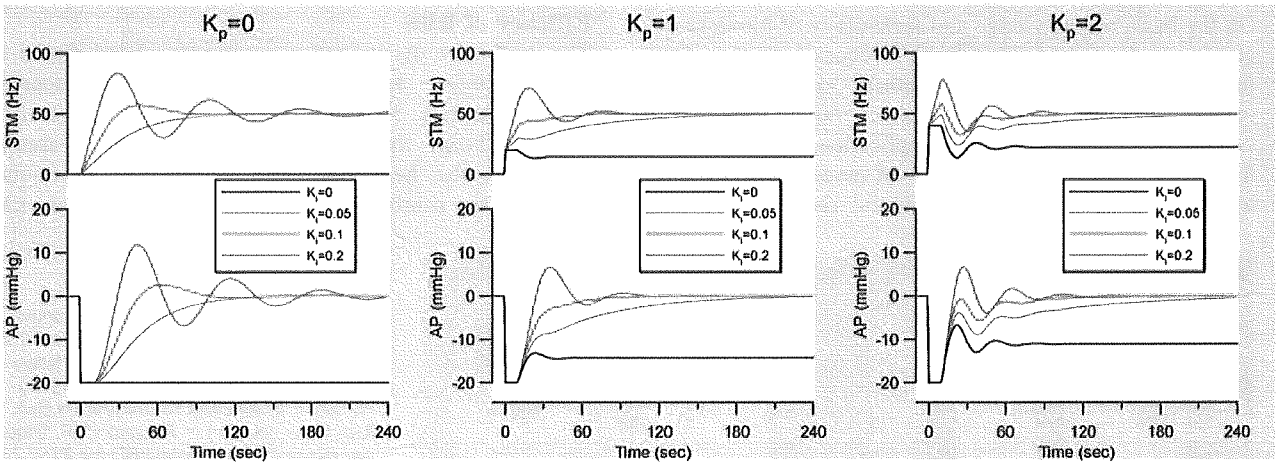

Figure 3. Numerical simulations of a feedback controller of the BBS. A stepwise pressure decline with an amplitude of 20 mm Hg is assumed to be imposed. Results are shown for 12 combinations of proportional (K_p) and integral (K_i) correction factors. See text for explanation.

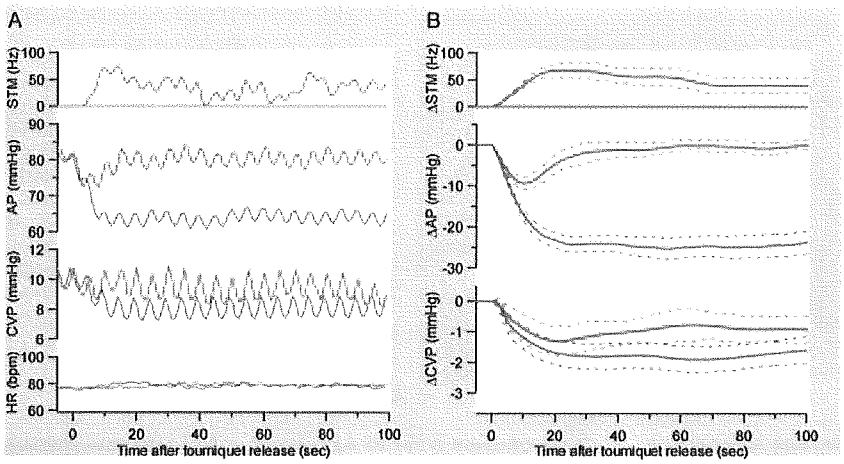

Figure 4. A, Representative example of original tracings of STM, AP, CVP, and heart rate (HR) during 2 episodes of rapid progressive hypotension induced by sudden deflation of a thigh tourniquet in a patient. When the BBS was inactive (blue line), AP decreased immediately after tourniquet release and did not return to baseline level. By contrast, when the BBS was activated (red line), the artificial vasomotor center automatically computed STM and drove an electrical stimulator to restore AP. B, Plots showing averaged changes in STM, AP, and CVP after tourniquet release among 21 patients. Data are expressed as mean (solid line)±SD (dotted line). See text for explanation.

deflation of the thigh tourniquet produced a rapid progressive fall in AP of ≈20 mm Hg within 10 seconds, while lowering CVP by 2 mm Hg. By contrast, when the BBS was activated, STM was computed automatically, and the spinal cord was stimulated appropriately to quickly and effectively attenuate the drop in AP and CVP. Figure 4B summarizes the results obtained from 21 patients, demonstrating effectiveness of the BBS performance in buffering the AP fall in response to the sudden release of the tourniquet. As demonstrated in Figure 5, tourniquet release resulted in an AP decrease of 17±3 mm Hg at 10 seconds, 25±2 mm Hg at 50 seconds, and 24±3 mm Hg at100 seconds. By contrast, during real-time execution of the BBS, the decrease in AP was 9±2 mm Hg at 10 seconds, 1±2 mm Hg at 50 seconds, and 0±1 mm Hg at 100 seconds after the deflation. These data indicated that the BBS significantly attenuated the decrease in AP at these 3 time points and nullified the hypotensive effect of tourniquet release within 50 seconds. Similarly, the BBS significantly suppressed the decrease in CVP within 50 seconds after the release of the tourniquet.

Discussion

Design of BBS

On the basis of knowledge and technology of bionics, we previously developed an artificial feedback control system for automatic regulation of sympathetic vasomotor tone in animal models of central baroreflex failure.[20–22] As a crucial first step to clinical application, we tested its feasibility and efficacy in a clinical model of orthostatic hypotension. A percutaneous epidural catheter approach was established for the monitoring of spinal function during surgery and for pain management,[28] and the lower thoracic level was selected for spinal cord stimulation based on earlier reports that the abdominal splanchnic vascular bed is a major effector mechanism for arterial baroreflex in animals[23,24] and humans.[25] Although the percutaneous epidural approach is less invasive than implantation surgery, spinal cord stimulation excites motor and sensory nerves[12,22,28] in addition to sympathetic vasomotor efferents. Therefore, administration of sufficient doses of muscle relaxants and analgesics was required during experimental protocols. Under these conditions, the dynamic response of AP to STM was easily characterized by the white noise system identification method. Furthermore, the quantitatively estimated results of transfer function analysis (Figure 2B) enabled simulation of the effects of feedback correction factors[27] on performance of the BBS. As demonstrated in Figure 3, the simulation results suggested that the specific combination of feedback correction factors could optimize the performance of the BBS. On the basis of these results, the feedback correction factors were determined to allow the BBS to quickly stabilize AP against the external disturbances.

Efficacy of BBS

The present study utilized a tourniquet-related model of hypotension[29–31] during general anesthesia[32,33] to approximate orthostatic hypotension due to central baroreflex failure. Except for the change in peripheral vascular resistance, the hemodynamic changes after tourniquet deflation are similar to those achieved after upright tilt-

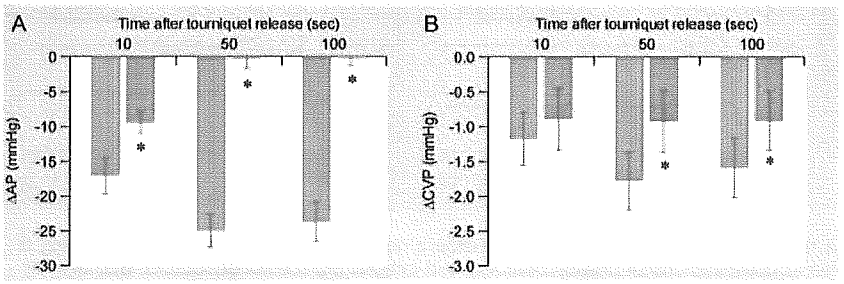

Figure 5. Bar graphs showing changes in AP (A) and CVP (B) at 10, 50, and 100 seconds after tourniquet release. Implementation of the BBS (red column) significantly attenuated tourniquet-related falls (blue column) in AP and CVP. Data are expressed as mean±SD for 21 patients. *Overall $P<0.05$.

ing.[29,31] For example, tourniquet release results in a rapid increase in venous pooling in the affected limb with a subsequent decrease in venous return and cardiac output. Under general anesthesia with volatile gases such as sevoflurane,[32,33] arterial baroreflex function is inhibited, and the hemodynamic disturbance produced by the tourniquet inevitably results in abrupt hypotension. In rare instances, tourniquet deflation can also trigger fatal circulatory collapse.[29]

Despite the fact that the BBS was implemented with fixed values of feedback correction factors for all patients, the BBS successfully stabilized AP against the hemodynamic challenge induced by sudden tourniquet release (Figure 4). These data indicate that the BBS may compensate for some individual differences in the dynamic response of AP to STM.

Finally, the CVP response to STM (Figure 4) in the present study suggests that the BBS attenuated a decrease in venous return. Previous studies have demonstrated that the baroreflex-mediated vasoconstriction in the splanchnic vascular bed is a major mechanism for recruitment of venous return during head-up tilting.[23,25] Therefore, the BBS may functionally mimic the baroreflex control of venous return and control of AP.

Study Limitations

This study possessed several limitations. First, based on the previous results[20–22] obtained from animal studies, the stimulation electrodes were placed in the epidural space at the level of the lower thoracic cord; however, further study to determine the optimal site of electrode placement would be of benefit. Second, it is unclear whether or not the feedback controller designed in the present study is universally applicable to other cases. Although preset parameters for feedback correction were used in the present study, other approaches based on a robust control theory could yield a better result. Finally, the epidural catheter method for sympathetic nerve stimulation is associated with significant pain and discomfort. Thus, practical use of the BBS requires an appropriate method for stimulating only efferent sympathetic nerves.

Clinical Implications

The present study confirmed the efficacy of the BBS in a clinical setting and suggests that the BBS has tremendous potential as a new therapeutic modality for treatment of severe orthostatic intolerance in patients with various syndromes of central baroreflex failure, including Shy-Drager syndrome, baroreceptor deafferentation, and traumatic spinal cord injuries.

Acknowledgments

This study was supported by a Health and Labor Sciences research grant (H14-NANO-002, H16-NANO-005, H15-KOKORO-019) from the Ministry of Health, Labor, and Welfare of Japan and by a grant-in-aid for scientific research (15300165) from the Ministry of Education, Science, Sports, and Culture of Japan.

Disclosures

None.

References

1. Guyton AC, Coleman TG, Granger HJ. Circulation: overall regulation. *Ann Rev Physiol.* 1972;34:13–46.
2. Robertson D. Diagnosis and management of baroreflex failure. *Primary Cardiol.* 1995;21:37–40.
3. Sunagawa K, Sato T, Kawada T. Integrative sympathetic baroreflex regulation of arterial pressure. *Ann N Y Acad Sci.* 2001;940:314–323.
4. Ketch T, Biaggioni I, Robertson R, Robertson D. Four faces of baroreflex failure: hypertensive crisis, volatile hypertension, orthostatic tachycardia, and malignant vagotonia. *Circulation.* 2002;105:2518–2523.
5. Sato T, Kawada T, Inagaki M, Shishido T, Takaki H, Sugimachi M, Sunagawa K. New analytical framework for understanding the sympathetic baroreflex control of arterial pressure. *Am J Physiol Heart Circ Physiol.* 1999;276:H2251–H2261.
6. Shy M, Drager GA. A neurological syndrome associated with orthostatic hypotension: a clinico-pathologic study. *Arch Neurol.* 1960;3:511–527.
7. The Consensus Committee of the American Autonomic Society and the American Academy of Neurology. Consensus statement on the definition of orthostatic hypotension, pure autonomic failure, and multiple system atrophy. *Neurology.* 1996;46:1470.
8. Schatz IJ. Farewell to the "Shy-Drager syndrome." *Ann Intern Med.* 1996;125:74–75.
9. Goldstein DS, Holmes C, Cannon RO III, Eisenhofer G, Kopin IJ. Sympathetic cardioneuropathy in dysautonomias. *N Engl J Med.* 1997;336:696–702.
10. Onrot J, Wiley RG, Fogo A, Biaggioni I, Robertson D, Hollister AS. Neck tumour with syncope due to paroxysmal sympathetic withdrawal. *J Neurol Neurosurg Psychiatry.* 1987;50:1063–1066.
11. Lee HT, Brown J, Fee WE Jr. Baroreflex dysfunction after nasopharyngectomy and bilateral carotid isolation. *Arch Otolaryngol Head Neck Surg.* 1997;123:434–437.
12. Frankel HL, Mathias CJ. Severe hypertension in patients with high spinal cord lesions undergoing electro-ejaculation: management with prostaglandin E_2. *Paraplegia.* 1980;18:293–299.
13. Matthews JM, Wheeler GD, Burnham RS, Malone LA, Steadward RD. The effects of surface anaesthesia on the autonomic dysreflexia response during functional electrical stimulation. *Spinal Cord.* 1997;35:647–651.
14. Wilcox CS, Puritz R, Lightman SL, Bannister R, Aminoff MJ. Plasma volume regulation in patients with progressive autonomic failure during changes in salt intake or posture. *J Lab Clin Med.* 1984;104:331–339.
15. Jordan J, Shannon JR, Diedrich A, Black B, Robertson D, Biaggioni I. Water potentiates the pressor effect of ephedra alkaloids. *Circulation.* 2004;109:1823–1825.
16. Kristinsson A. Programmed atrial pacing for orthostatic hypotension. *Acta Med Scand.* 1983;214:79–83.
17. Bannister R, da Costa DF, Hendry WG, Jacobs J, Mathias CJ. Atrial demand pacing to protect against vagal overactivity in sympathetic autonomic neuropathy. *Brain.* 1986;109:345–356.
18. Kachi T, Iwase S, Mano T, Saito M, Kunimoto M, Sobue I. Effect of L-threo-3,4-dihydroxyphenylserine on muscle sympathetic nerve activities in Shy-Drager syndrome. *Neurology.* 1988;38:1091–1094.
19. Obara A, Yamashita H, Onodera S, Yahara O, Honda H, Hasebe N. Effect of xamoterol in Shy-Drager syndrome. *Circulation.* 1992;85:606–611.
20. Sato T, Kawada T, Shishido T, Sugimachi M, Alexander J Jr, Sunagawa K. Novel therapeutic strategy against central baroreflex failure: a bionic baroreflex system. *Circulation.* 1999;100:299–304.
21. Sato T, Kawada T, Sugimachi M, Sunagawa K. Bionic technology revitalizes native baroreflex function in rats with baroreflex failure. *Circulation.* 2002;106:730–734.
22. Yanagiya Y, Sato T, Kawada T, Inagaki M, Tatewaki T, Zheng C, Kamiya A, Takaki H, Sugimachi M, Sunagawa K. Bionic epidural stimulation restores arterial pressure regulation during orthostasis. *J Appl Physiol.* 2004;97:984–990.
23. Hainsworth R, Karim F. Responses of abdominal vascular capacitance in the anaesthetized dog to changes in carotid sinus pressure. *J Physiol Lond.* 1976;262:659–677.

24. Carneiro JJ, Donald DE. Blood reservoir function of dog spleen, liver, and intestine. *Am J Physiol Heart Circ Physiol.* 1977;232:H67–H72.
25. Minson CT, Wladkowski SL, Pawelczyk JA, Kenney WL. Age, splanchnic vasoconstriction, and heat stress during tilting. *Am J Physiol Regul Integr Comp Physiol.* 1999;276:R203–R212.
26. Marmarelis PZ, Marmarelis VZ. *Analysis of Physiological Systems: The White-Noise Approach.* New York, NY: Plenum; 1978.
27. Kawada T, Sunagawa G, Takaki H, Shishido T, Miyano H, Miyashita H, Sato T, Sugimachi M, Sunagawa K. Development of a servo-controller of heart rate using treadmill. *Jpn Circ J.* 1999;63:945–950.
28. Shimoji K, Hokari T, Kano T, Tomita M, Kimura R, Watanabe S, Endoh H, Fukuda S, Fujiwara N, Aida S. Management of intractable pain with percutaneous epidural spinal cord stimulation: differences in pain-relieving effects among diseases and sites of pain. *Anesth Analg.* 1993;77:110–116.
29. Kahn RL, Marino V, Urquhart B, Sharrock NE. Hemodynamic changes associated with tourniquet use under epidural anesthesia for total knee arthroplasty. *Reg Anesth.* 1992;17:228–232.
30. Feldman DL, Wigod M, Barwick W, Levin LS. Tourniquet-related hypotension in venous stasis ulcer excision. *Ann Plast Surg.* 1993;30:556–559.
31. Sander-Jensen K, Mehlsen J, Secher NH, Bach FW, Bie P, Giese J, Schwartz TW, Trap-Jensen J, Warberg J. Progressive central hypovolaemia in man–resulting in a vasovagal syncope? Haemodynamic and endocrine variables during venous tourniquets of the thighs. *Clin Physiol.* 1987;7:231–242.
32. Tanaka M, Nishikawa T. Arterial baroreflex function in humans anaesthetized with sevoflurane. *Br J Anaesth.* 1999;82:350–354.
33. Keyl C, Schneider A, Hobbhahn J, Bernardi L. Sinusoidal neck suction for evaluation of baroreflex sensitivity during desflurane and sevoflurane anesthesia. *Anesth Analg.* 2002;95:1629–1636.

CLINICAL PERSPECTIVE

Central baroreflex failure due to Shy-Drager syndrome, baroreceptor deafferentation, and traumatic spinal cord injuries results in severe orthostatic hypotension. However, most commonly used interventions, such as salt loading, cardiac pacing, and pharmacological approaches, can neither restore nor reproduce the functioning of a native vasomotor center. Here, we proposed a novel therapeutic strategy against central baroreflex failure and developed a bionic baroreflex system (BBS). The BBS consisted of a pressure sensor, computer, electrical stimulator, and epidural catheter with sympathetic nerve stimulation electrodes. While automatically calculating the frequency of a pulse train in response to a change in arterial pressure, the computer drove the stimulator at the appropriate frequency to stabilize arterial pressure against an external disturbance. According to a parametric negative-feedback control theory, we designed an algorithm of the computer functioning as an artificial vasomotor center. The efficacy of the BBS was tested in a clinical model of orthostatic hypotension during knee joint surgery. Without the implementation of the BBS, a sudden deflation of a thigh tourniquet resulted in rapid progressive hypotension. By contrast, during real-time execution of the BBS, arterial pressure was quickly restored to the baseline level before tourniquet release. These results suggest the technical feasibility of functional restoration of arterial baroreflex with the BBS.

J Appl Physiol 100: 1278–1286, 2006.
First published December 22, 2005; doi:10.1152/japplphysiol.01206.2005.

TRANSLATIONAL PHYSIOLOGY

Automated drug delivery system to control systemic arterial pressure, cardiac output, and left heart filling pressure in acute decompensated heart failure

Kazunori Uemura,[1] Atsunori Kamiya,[1] Ichiro Hidaka,[1] Toru Kawada,[1] Shuji Shimizu,[1] Toshiaki Shishido,[1] Makoto Yoshizawa,[2] Masaru Sugimachi,[1] and Kenji Sunagawa[3]

[1]*Department of Cardiovascular Dynamics, National Cardiovascular Center Research Institute, Suita;* [2]*Research Division on Advanced Information Technology, Information Synergy Center, Tohoku University, Sendai;* [3]*Department of Cardiovascular Medicine, Kyushu University Graduate School of Medical Science, Fukuoka, Japan*

Submitted 22 September 2005; accepted in final form 17 December 2005

Uemura, Kazunori, Atsunori Kamiya, Ichiro Hidaka, Toru Kawada, Shuji Shimizu, Toshiaki Shishido, Makoto Yoshizawa, Masaru Sugimachi, and Kenji Sunagawa. Automated drug delivery system to control systemic arterial pressure, cardiac output, and left heart filling pressure in acute decompensated heart failure. *J Appl Physiol* 100: 1278–1286, 2006. First published December 22, 2005; doi:10.1152/japplphysiol.01206.2005.—Pharmacological support with inotropes and vasodilators to control decompensated hemodynamics requires strict monitoring of patient condition and frequent adjustments of drug infusion rates, which is difficult and time-consuming, especially in hemodynamically unstable patients. To overcome this difficulty, we have developed a novel automated drug delivery system for simultaneous control of systemic arterial pressure (AP), cardiac output (CO), and left atrial pressure (Pla). Previous systems attempted to directly control AP and CO by estimating their responses to drug infusions. This approach is inapplicable because of the difficulties to estimate simultaneous AP, CO, and Pla responses to the infusion of multiple drugs. The circulatory equilibrium framework developed previously (Uemura K, Sugimachi M, Kawada T, Kamiya A, Jin Y, Kashihara K, and Sunagawa K. *Am J Physiol Heart Circ Physiol* 286: H2376–H2385, 2004) indicates that AP, CO, and Pla are determined by an equilibrium of the pumping ability of the left heart (S_L), stressed blood volume (V), and systemic arterial resistance (R). Our system directly controls S_L with dobutamine, V with dextran/furosemide, and R with nitroprusside, thereby controlling the three variables. We evaluated the efficacy of our system in 12 anesthetized dogs with acute decompensated heart failure. Once activated, the system restored S_L, V, and R within 30 min, resulting in the restoration of normal AP, CO, and Pla. Steady-state deviations from target values were small for AP [4.4 mmHg (SD 2.6)], CO [5.4 $ml \cdot min^{-1} \cdot kg^{-1}$ (SD 2.4)] and Pla [0.8 mmHg (SD 0.6)]. In conclusion, by directly controlling the mechanical determinants of circulation, our system has enabled simultaneous control of AP, CO, and Pla with good accuracy and stability.

computers; negative feedback; circulatory equilibrium

IN THE MANAGEMENT OF PATIENTS with acute decompensated heart failure after myocardial infarction or after cardiac surgical procedures, cardiovascular agents such as inotropes and/or vasodilators are commonly used to control systemic arterial pressure (AP), cardiac output (CO), and left heart filling pressure (2, 13, 20). Because responses to these agents vary between patients and within patient over time, strict monitoring of patient condition and frequent adjustments of drug infusion rates are usually required. This is a difficult and time-consuming process, especially in hemodynamically unstable patients. Several closed-loop systems to automate drug infusion have been developed to facilitate this process (10, 11, 18, 26, 27). Closed-loop control of AP with vasodilators was more precise and stable than manual controls (10, 11). Chitwood et al. (10) demonstrated that, compared with manual control, closed-loop control of postoperative hypertension significantly improves patient outcome by reducing the transfusion requirement and postoperative blood loss. Although closed-loop control of hemodynamics has been suggested to be useful in clinical settings, no closed-loop system so far developed is capable of controlling the overall hemodynamics; i.e., controlling AP, CO, and left heart filling pressure simultaneously (18). This is because all previous systems attempted to directly control the hemodynamic variable by estimating response of the variable to drug infusion (10, 11, 18, 26, 27). Although such an approach worked well in controlling a single variable, it cannot be applied to control of the three variables, because it is difficult to simultaneously estimate their responses to the infusions of multiple drugs.

In this study, we developed a new automated drug delivery system that is capable of controlling AP, CO, and left atrial pressure (Pla). We modeled the entire cardiovascular system by extending Guyton's framework of circulatory equilibrium (16, 17, 24, 25). As shown in Fig. 1, the extended framework consists of an integrated cardiac output curve characterizing the pumping ability of the left and the right heart and a venous return surface characterizing the venous return property of the systemic and pulmonary circulation (24, 25). The intersection point of the integrated CO curve and the venous return surface predicts the equilibrium point of CO, Pla, and right atrial pressure (Pra) (Fig. 1) (24, 25). Once CO, Pla, and Pra are predicted from the intersection point, systemic arterial resistance determines AP. On the basis of this framework, instead of directly controlling AP, CO, and Pla, our system controls the integrated CO curve with dobutamine (Dob), the venous return surface with 10% dextran 40 (Dex) and furosemide (Fur), and systemic arterial resistance with sodium nitroprusside (SNP), thereby controlling the three hemodynamic variables.

Address for reprint requests and other correspondence: K. Uemura, Dept. of Cardiovascular Dynamics, National Cardiovascular Center Research Institute, 5-7-1 Fujishirodai, Suita 565-8565, Japan (e-mail: kuemura@ri.ncvc.go.jp).

The costs of publication of this article were defrayed in part by the payment of page charges. The article must therefore be hereby marked "*advertisement*" in accordance with 18 U.S.C. Section 1734 solely to indicate this fact.

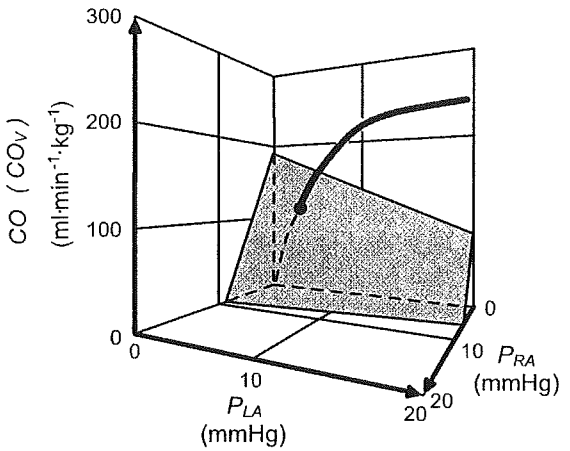

Fig. 1. Diagram of circulatory equilibrium for cardiac output (CO), venous return (CO_V), left atrial pressure (Pla), and right atrial pressure (Pra). The equilibrium CO, Pla, and Pra are obtained as the intersection point of the venous return surface and integrated cardiac output curve. [Modified from Uemura et al. (Ref 25).]

The purpose of this study was, therefore, to develop and validate the new automated drug delivery system. We evaluated the efficacy of our system in a canine model of acute ischemic heart failure. Our results indicated that this novel automated drug delivery system was able to control AP, CO, and Pla simultaneously with reasonably good accuracy and stability.

METHODS

Cardiac Output Curve, Venous Return Surface, and Arterial Resistance

On the basis of previous studies, we parameterized the integrated CO curve by the pumping ability of the left heart (S_L), the venous return surface by total stressed blood volume (V), and the systemic arterial resistance by R (see APPENDIX A) (24, 25). Our system aims to control these cardiovascular parameters to achieve target AP (AP*), target CO (CO*), and target Pla (Pla*).

Automated Drug Delivery System

Figure 2*A* illustrates a block diagram of the automated drug delivery system, using a negative feedback mechanism.

Target values of S_L (S_L*), V (V*), and R (R*) are determined according to the AP*, CO*, and Pla* (see APPENDIX B). The subject's S_L, V, and R are calculated from the measured AP, CO, Pla, and Pra (Fig. 2*A*). S_L, V, and R are compared with S_L*, V*, and R*, respectively.

To minimize the difference between S_L* and S_L ($\Delta S_L = S_L^* - S_L$) and the difference between R* and R ($\Delta R = R^* - R$), proportional-integral (PI) feedback controllers adjusts infusion rates of Dob and SNP, respectively (Fig. 2*A*). In the PI controller (Fig. 2*B*), ΔS_L (or ΔR) and the difference integrated with an integral gain (K_i) are summed and scaled by a proportional gain (K_p) to give the infusion rate of Dob (or SNP). We determined values of K_i and K_p on the

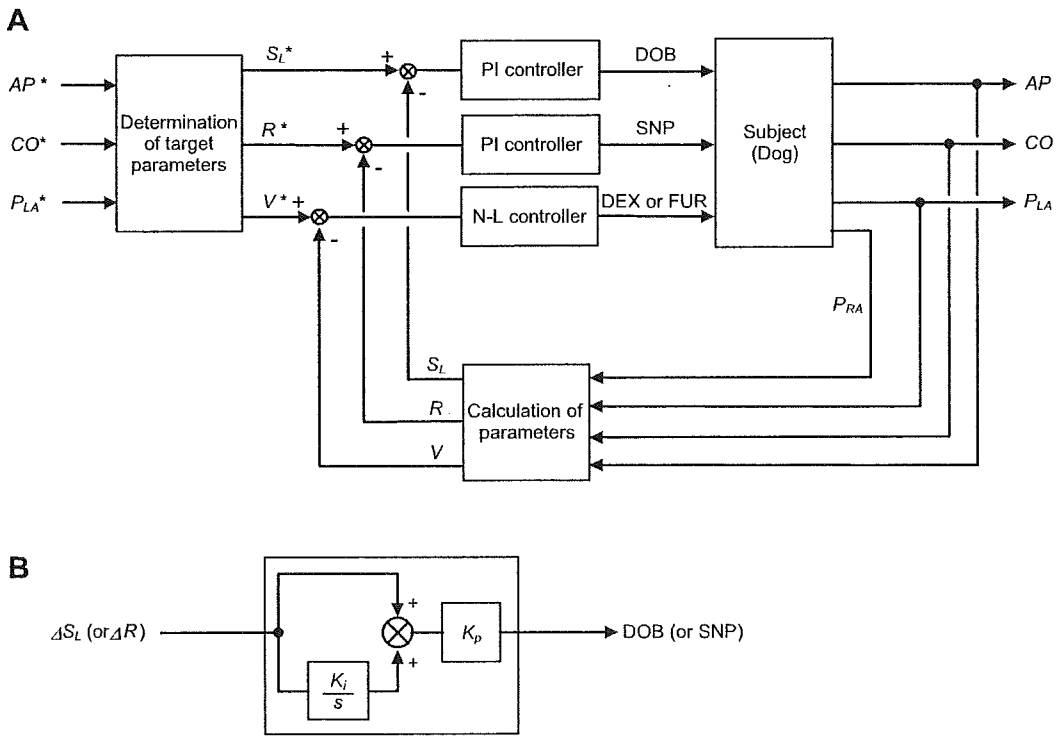

Fig. 2. *A*: block diagram of an automated drug delivery system for simultaneous control of systemic arterial pressure (AP), CO, and Pla. AP*, CO* and Pla* represent target AP, target CO, and target Pla, respectively. From these target variables, target values of pumping ability of the left heart (S_L*), stressed blood volume (V*), and systemic arterial resistance (R*) are determined. Subject's S_L, V, and R are calculated from measured AP, CO, Pla, and Pra. Proportional-integral (PI) controllers adjust infusion rate of dobutamine (Dob) and sodium nitroprusside (SNP) to minimize the difference between S_L and S_L* (ΔS_L), and the difference between R and R* (ΔR), respectively. Nonlinear (N-L) controller adjusts infusion of 10% dextran 40 (Dex) or injection of furosemide (Fur) so that the difference between V and V* is minimized. *B*: block diagram of the PI controller. K_i and K_p represent the integral and proportional gain constants, respectively; s is a Laplace operator.

basis of open-loop response of S_L (or R) to the infusion of Dob (or SNP) (4, 9).

To minimize the difference between V* and V ($\Delta V = V^*-V$), a nonlinear (NL) feedback controller (Fig. 2*A*) adjusts the infusion of Dex or injection of Fur on the basis of the following "if-then" rules:

Rule 1: If $\Delta V \geq X_1$ ml/kg then infuse Dex (Y_1, ml/min)

Rule 2: If $\Delta V \leq X_2$ ml/kg then inject Fur (Y_2, mg)

We determined values of X_1, Y_1, X_2, and Y_2 on the basis of the open-loop response of V to the infusion of Dex and Fur.

These adjustment processes are repeated in parallel and continued until the differences disappear.

Preparation

We used 35 adult mongrel dogs in this study [both sexes, body weight 25 kg (SD 4)]. Care of the animals was in strict accordance with the guiding principles of the Physiological Society of Japan. All protocols were approved by the Animal Subjects Committee of the National Cardiovascular Center. Anesthesia was induced with pentobarbital sodium (25 mg/kg). Animals were intubated endotracheally. Isoflurane (1.0%) was inhaled continuously to maintain an appropriate level of anesthesia during the experiment. A catheter (8-Fr) was placed in the right femoral artery, which was connected to a pressure transducer (DX-200, Nihon Kohden, Tokyo, Japan) to measure AP. After a median sternotomy, a small pericardial incision was made at the level of the aortic root. Through the incision, an ultrasonic flow meter (20A594, Transonics, Ithaca, NY) was placed around the ascending aorta to measure CO. Fluid-filled catheters were placed in the left and right atria to measure Pla and Pra, respectively. They were connected to pressure transducers (DX-200, Nihon Kohden). The junction between the vena cavae and the right atrium was taken as the reference point for zero pressure. The undamped natural frequency and the damping ratio of the fluid filled catheters for the pressure measurements were 21 Hz and 0.22, respectively. A urinary catheter was inserted to measure urine volume.

A catheter (6-Fr) was placed in the right femoral vein. A roller pump (Minipuls 3, Gilson, Middleton, WI) was attached to the venous line to infuse Dex. A double-lumen catheter was also introduced into the right femoral vein for administration of Dob and SNP. Infusion pumps (CFV-3200, Nihon Kohden) were used for Dob and SNP infusion. The infusion rates of Dex, Dob, and SNP were controlled with a personal computer (MA20V, NEC, Tokyo, Japan) through a 12-bit digital-to-analog converter (DA12-8PCI, Contec, Osaka, Japan). A catheter (6-Fr) was placed in the right external jugular vein, from which Fur was injected after a command signal from the computer.

Experimental Protocols

We induced left ventricular failure (LVF) in all the animals by embolizing the left circumflex coronary artery with glass microspheres (90 μm in diameter) (24, 25). We adjusted the amount of injected microspheres to increase Pla to more than 18 mmHg or decrease CO to less than 70 $ml \cdot min^{-1} \cdot kg^{-1}$. When ventricular tachycardia or frequent premature ventricular contractions were noted, lidocaine (1 mg/min) was infused to suppress the arrhythmia.

Response of cardiovascular parameters to drug infusion. Under open-loop conditions, we examined the response of cardiovascular parameters to drug infusions in 21 dogs with LVF. In 10 dogs, we infused Dob in a stepwise manner at 6 $\mu g \cdot kg^{-1} \cdot min^{-1}$ for 10 min to obtain a step response of S_L. In six dogs, we infused SNP at 2 $\mu g \cdot kg^{-1} \cdot min^{-1}$ for 10 min to obtain a step response of R. In five dogs, we infused Dex at 0.4 $ml \cdot min^{-1} \cdot kg^{-1}$ for 10 min to observe the response of V. In seven dogs, we injected Fur (20 mg, bolus iv) and observed the response of V and urine volume for 50 min.

Application of the automated drug delivery system. We applied the system to the other 14 dogs with LVF. We first defined AP* (90–105 mmHg), CO* (90–100 $ml \cdot min^{-1} \cdot kg^{-1}$), and Pla* (8–12 mmHg), which were fed into the system to determine S_L*, V*, and R* (see APPENDIX B). The controllers were then activated by closing the loops. In 12 dogs (*group 1*), we observed the performance of the system over 50–60 min. In two dogs (*group 2*), we observed the performance of the system over 100–150 min to evaluate stability of the closed-loop control over a longer periods of time.

With the use of the computer, analog signals of AP, CO, Pla, and Pra were digitized at 200 Hz with a 12-bit analog-to-digital converter [AD12-16U(PCI)E, Contec, Osaka, Japan] and stored on a hard disk for offline analysis. In the closed-loop control, the digitized signals were smoothed by a low-pass filter (time constant, 10 s) and were used as the system controlled variables. The infusion rates of Dob, SNP, and Dex were also stored. Urine volume after the injection of Fur was recorded.

Data Analysis

Evaluation of the response of cardiovascular parameters and design of the controller. We described the step response of S_L and R by a transfer function of a first-order model with a transport delay. In this model, change in S_L from baseline (δS_L) in response to Dob infusion can be expressed by the following formula:

$$\delta S_L(t) = \begin{cases} G \cdot \left[1 - \exp\left(-\dfrac{t-L}{T}\right)\right] & (t \geq L) \\ 0 & (t < L) \end{cases} \qquad (1)$$

where G is static gain [$ml \cdot min^{-1} \cdot kg^{-1} (\mu g \cdot kg^{-1} \cdot min^{-1})^{-1}$], L is transport delay (s), and T is time constant (s). Change in R from baseline (δR) in response to the SNP infusion can be expressed similarly and is characterized by G [$mmHg \cdot min \cdot ml^{-1} \cdot kg (\mu g \cdot kg^{-1} \cdot min^{-1})^{-1}$], L (s), and T (s). We estimated the parameters of the transfer function by approximating δS_L and δR to *Eq. 1* using the least square method. We averaged the parameters of the transfer function of S_L response for 10 animals and those of R response for 6 animals. The averaged parameters were used to determine the PI gain constants, K_I and K_P, in accordance with the method of Chien et al. (9). Their method provides PI constants that permit the regulated variable to respond rapidly without overshoot (4, 9).

We evaluated the change in V from baseline (δV) in response to the infusion of Dex and Fur. On the basis of δV, we determined the constants (X_1, Y_1, X_2, and Y_2) of the if-then rules.

Efficacy of the automated drug delivery system. We calculated the following indexes to evaluate the accuracy and stability of the control of AP, CO, and Pla by the new system: the time required for the hemodynamic variables to reach the acceptable ranges of the target values (±10 mmHg for AP, ±10 $ml \cdot min^{-1} \cdot kg^{-1}$ for CO, ±2 mmHg for Pla), and the standard deviations of the steady-state differences between AP and AP*, between CO and CO*, and between Pla and Pla*. Because steady states were reached within 30 min in all the variables in the present study, standard deviations were calculated from 30 min after the loop was closed.

Statistics

Group data are expressed as means (SD) unless otherwise stated. Student's paired *t*-test was used to compare hemodynamic data at baseline and after the coronary embolization. One-way ANOVA with Tukey's post hoc test was used to compare hemodynamic data before, during, and after the closed-loop control of hemodynamics. The level of statistical significance was defined as $P < 0.05$.

RESULTS

Hemodynamic data at baseline and after left circumflex coronary artery embolization are summarized in Table 1. Coronary embolization more than doubled Pla [from 7.5 (SD 1.9) to 19.4 (SD 6.2) mmHg] and halved CO [from 131.4 (SD

Table 1. *Hemodynamic data at baseline and after left circumflex coronary artery embolization*

	Baseline	Embolization
HR, beats/min	141.3 (19.5) [112.0–188.3]	146.2 (28.8) [81.4–197.9]
AP, mmHg	109.1 (18.7) [76.4–140.0]	90.9 (16.5) [66.9–135.6]*
CO, ml·min^{-1}·kg^{-1}	131.4 (40.9) [64.5–229.2]	66.8 (23.3) [30.3–121.7]*
Pla, mmHg	7.5 (1.9) [4.7–12.8]	19.4 (6.2) [7.9–34.5]*
Pra, mmHg	4.2 (1.2) [2.1–7.2]	6.0 (1.8) [3.5–9.9]*
S_L, ml·min^{-1}·kg^{-1}	54.3 (18.1) [25.2–105.9]	19.1 (7.6) [8.0–33.7]*
R, mmHg·min·ml^{-1}·kg	0.9 (0.4) [0.4–1.8]	1.4 (0.5) [0.7–2.6]*
V, ml/kg	31.0 (6.6) [21.7–45.2]	32.3 (4.9) [20.6–43.7]

Values are means (SD) (n = 35 in each group). Numbers in brackets are the ranges. HR, heart rate. AP, systemic arterial pressure; CO, cardiac output; Pla, left atrial pressure; Pra, right atrial pressure; S_L, pumping ability of the left heart; R, systemic arterial resistance; V, stressed blood volume. *P < 0.01 vs. baseline.

40.9) to 66.8 (SD 23.3) ml·min^{-1}·kg^{-1}]. This decreased S_L to about one-third of the baseline value, which indicates substantial downward shift of the left cardiac output curve. These changes are compatible with severe LVF.

Response of Cardiovascular Parameters to Drug Infusion

Figure 3 shows the open-loop responses of cardiovascular parameters to drug infusions. Figure 3, *A* and *B*, shows the averaged time course of δS_L during Dob infusion (n = 10) and that of δR during SNP infusion (n = 6), respectively. Dob infusion increased δS_L, and SNP infusion decreased δR exponentially. The results of the fit of δS_L and δR to *Eq. 1* are summarized in Table 2. The fact that the correlation coefficients were close to unity, with a small standard error of the estimate relative to the amount of δS_L and δR, suggested that the approximation of δS_L and δR to *Eq. 1* was reasonably accurate. On the basis of the averaged parameters of the transfer function (Table 2), we determined the PI gain constants for Dob infusion [K_i = 0.01 s^{-1}, K_p = 0.06 μg·kg^{-1}·min^{-1} (ml·min^{-1}·kg^{-1})$^{-1}$] and for SNP infusion [K_i = 0.007 s^{-1}, K_p = −1.37 μg·kg^{-1}·min^{-1} (mmHg·min·ml^{-1}·kg)$^{-1}$].

Figure 3*C* shows the averaged time course of δV in response to Dex infusion (n = 5). δV increased and plateaued [7.2 ml/kg (SD 2.2)] after the cessation of Dex infusion. δV at the plateau was greater than the total volume of Dex infused (4 ml/kg), suggesting transvascular fluid absorption by colloid osmotic pressure (3). Figure 3*D* shows the averaged time course of δV after a single intravenous injection of Fur (20 mg, n = 7). δV gradually decreased and reached a trough [−4.3 ml/kg (SD 3.5)] around 30 min after the Fur injection. Average urine volume was 180 ml (SD 94). On the basis of these responses, we determined the constants of the if-then rules as X_1 = 1 ml/kg, Y_1 = 10 ml/min, X_2 = −2 ml/kg, and Y_2 = 10 mg. To avoid oscillation between hypovole-

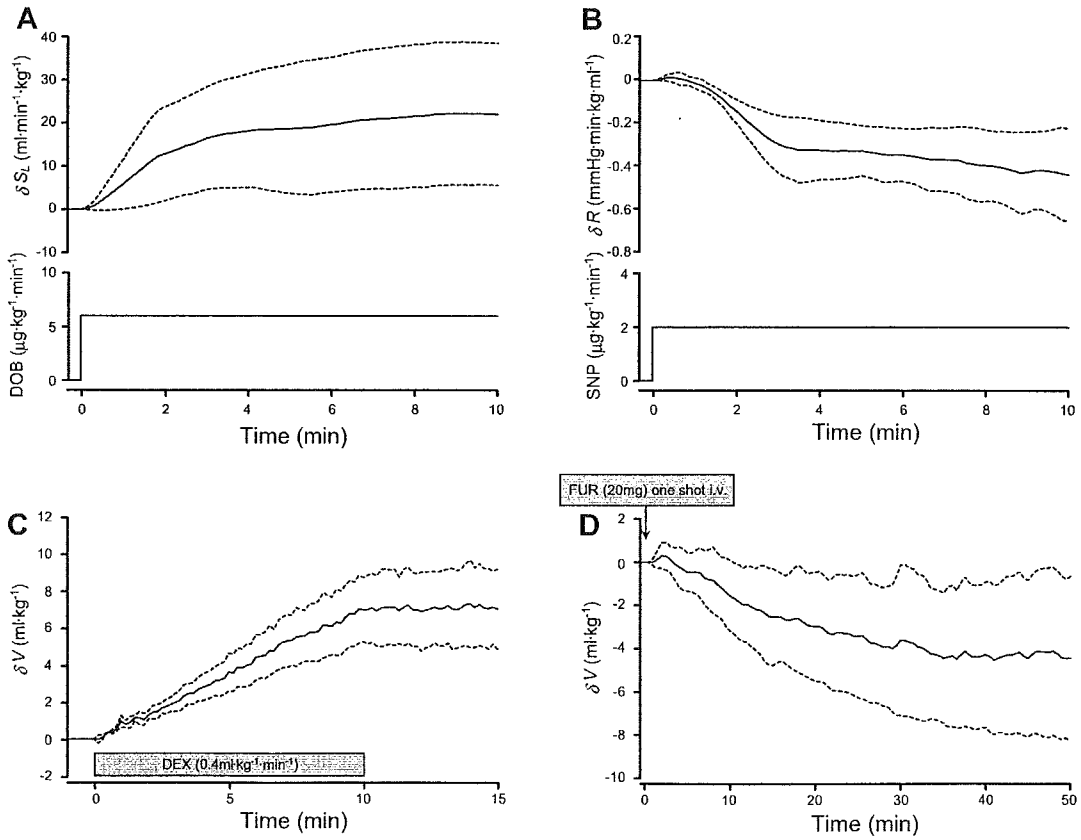

Fig. 3. Response of cardiovascular parameter to drug infusion. *A*: averaged response of S_L to stepwise Dob infusion (6 μg·kg^{-1}·min^{-1}) (n = 10). The ordinate indicates change in S_L from baseline (δS_L). *B*: averaged response of R to stepwise SNP infusion (2 μg·kg^{-1}·min^{-1}) (n = 6). The ordinate indicates change in R from baseline (δR). *C* and *D*: averaged response of V to Dex infusion (0.4 ml·min^{-1}·kg^{-1}) (*C*, n = 5) and to Fur (20 mg) injection (*D*, n = 7). The ordinates indicate change in V from baseline (δV). Data are expressed by mean (solid line) ± SD (broken line).

Table 2. *Parameters of step response of S_L and R*

	G	*L*	*T*	*r*	SEE
δS_L	3.6 (2.7)	63.5 (46.9)	79.0 (78.0)	0.91 (0.09)	2.0 (0.7)
δR	−0.21 (0.08)	69.8 (26.1)	117.1 (80.2)	0.93 (0.02)	0.06 (0.02)

Values are means (SD). δS_L, change in S_L from baseline; δR, change in R from baseline; *G*, static gain of δS_L [ml·min^{-1}·kg^{-1} (μg·kg^{-1}·min^{-1})$^{-1}$] and of δR [mmHg·min·ml^{-1}·kg (μg· kg^{-1}·min^{-1})$^{-1}$]; *L*, transport delay (s); *T*, time constant (s); *r*, correlation coefficient; SEE, standard error of the estimate of δS_L (ml·min^{-1}·kg^{-1}) and of δR (mmHg·min·ml^{-1}·kg).

mia and hypervolemia (hence infusion of Dex and injection of Fur), we introduced a dead zone (-2 ml/kg $< \Delta V <$ 1 ml/kg) into the rules (4). We set continuous checking for *rule 1* and checking at 20-min intervals for *rule 2*.

With the controllers thus designed, we evaluated the performance of the automated system in the next protocol.

Performance of the Automated Drug Delivery System

Figure 4 shows the experimental trial in a representative case. The automated system was activated at 0 min. Figure 4*A* shows the time courses of the infusion rates of Dob and SNP and the accumulated volume of infused Dex. In this case, Fur was not injected. Figure 4*B* shows the time courses of S_L, R, and V. Infusion rates of Dob, SNP, and Dex were adjusted so that S_L, R, and V reached their respective target values. By controlling the cardiovascular parameters, the automated system controlled AP, CO, and Pla accurately and stably as demonstrated in Fig. 4*C*. AP, CO, and Pla reached their respective target levels within 30 min and remained at these levels.

Figure 5 summarizes the results obtained for 12 dogs (*group 1*), demonstrating the effectiveness of the performance of the automated system. Figure 5*A* shows averaged time courses of the infusion rates of Dob and SNP, and the accumulated volume of infused Dex. The average infusion rates of Dob and SNP were 4.7 μg·kg^{-1}·min^{-1} (SD 2.6) and 4.2 μg·kg^{-1}·min^{-1} (SD 1.8), respectively. The average volume of infused Dex was 2.4 ml/kg (SD 1.9). Fur was injected once in one animal and twice in another animal. In these two animals, V decreased by 3.8–10.2 ml/kg in response to the injection of Fur with a total urine volume of 250–300 ml. Figure 5*B* shows averaged time courses of difference between S_L and S_L* ($S_L - S_L$*), difference between R and R* (R − R*), and difference between V and V* (V − V*). Once the system was activated, these differences rapidly converged to the zero lines in all the animals. S_L was restored to subnormal conditions [33.0 ml·min^{-1}·kg^{-1} (SD 2.6)] irrespective of the magnitude of depression before the control [13.8 ml·min^{-1}·kg^{-1} (SD 3.5), from 9.4 to 20.5 ml·min^{-1}·kg^{-1}]. These resulted in accurate and stable control of AP, CO, and Pla (Fig. 5*C*). The ordinates of Fig. 5*C* indicate the difference between AP and AP* (AP − AP*), difference between CO and CO* (CO − CO*), and difference between Pla and Pla* (Pla − Pla*). These differences also converged to the zero lines rapidly. The average times for AP, CO, and Pla to reach the acceptable ranges were 5.2 min (SD 6.6), 6.8 min (SD 4.6), and 11.7 min (SD 9.8),

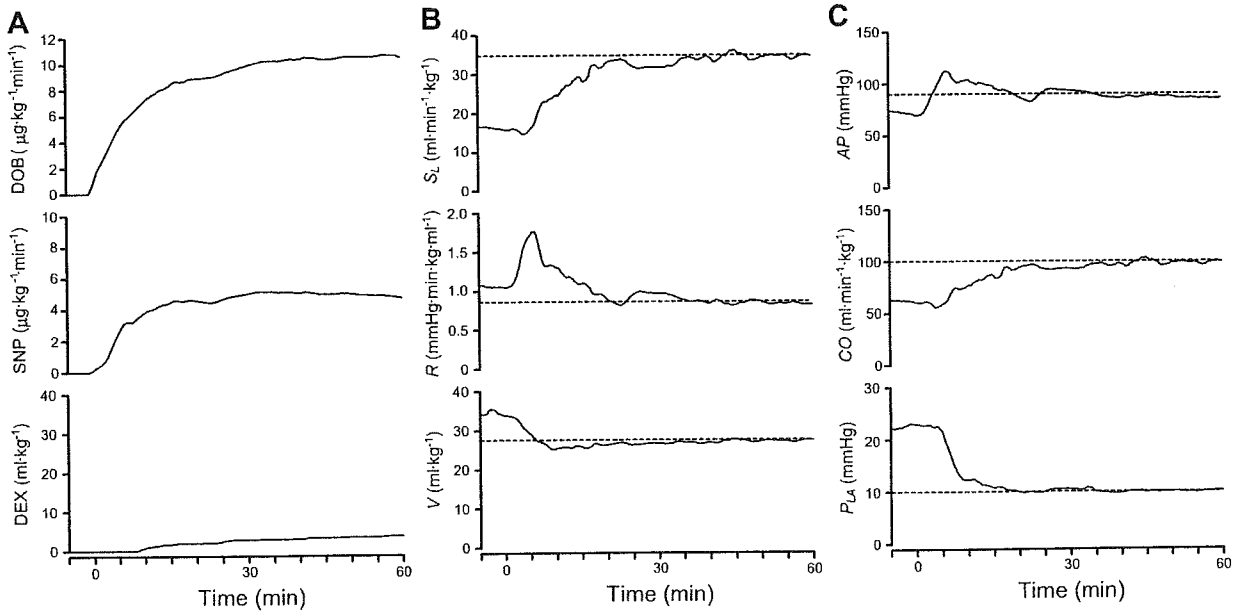

Fig. 4. Time courses of infusion rates of Dob and SNP, and cumulated volume of infused Dex (*A*), cardiovascular parameters (*B*), and hemodynamic variables (*C*) in 1 representative animal during closed-loop control of hemodynamics. Broken horizontal lines in *B* indicate target parameters (*top*, S_L*; *middle*, R*; *bottom*, V*). Broken horizontal lines in *C* indicate target hemodynamic variables (*top*, AP*; *middle*, CO*; *bottom*, Pla*). Drug infusion rates were adjusted so that the cardiovascular parameters reached the respective target values. As the parameters got closer to their targets, all 3 hemodynamic variables approached their respective target values.

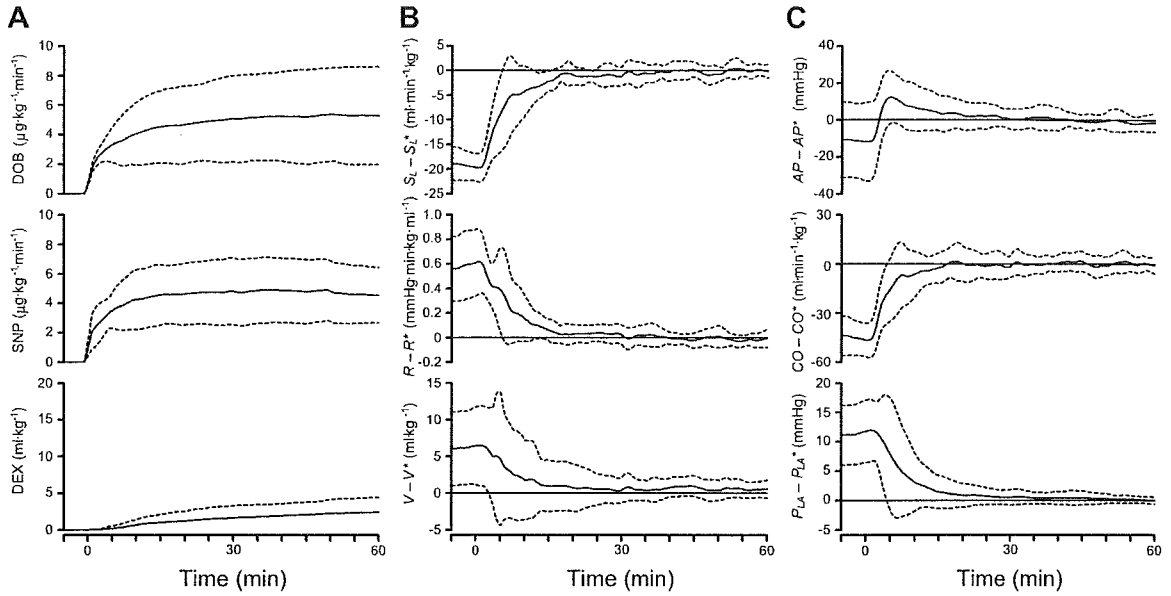

Fig. 5. Time courses of infusion rates of Dob and SNP, and cumulated volume of infused Dex (*A*), differences between measured and target cardiovascular parameters (*B*), and differences between measured and target hemodynamic variables (*C*) averaged for 12 dogs during closed-loop control of hemodynamics. Data are expressed as mean (solid line) ± SD (broken line). As the differences between measured and target parameters converged to the zero lines, the differences between measured and target hemodynamic variables also converged to the zero lines and remained at those levels.

respectively. The average standard deviations from the target values were small for AP [4.4 mmHg (SD 2.6)], CO [5.4 ml·min^{-1}·kg^{-1} (SD 2.4)] and Pla [0.8 mmHg (SD 0.6)]. In case of severe hypotension, restoring normal AP should be done within a few minutes to prevent cerebral ischemia. Four of 12 dogs exhibited severe hypotension [AP, 67 mmHg (SD 6)]. In these animals, AP* [95 mmHg (SD 4)] was attained within 4 min [mean 2.8 min (SD 0.7)]. Hemodynamic data before, during, and after the closed-loop control of hemodynamics are summarized in Table 3. After the system was turned off, AP, CO, and Pla gradually returned to their precontrol levels in 11 animals. In one animal, however, progressive hypotension followed by intractable ventricular fibrillation occurred ~3 min after the system was turned off.

In two dogs (*group 2*), AP, CO, and Pla were controlled with reasonable stability over a longer periods of time (100–150 min). Standard deviations from target values were small for AP (3.9–7.8 mmHg), CO (2.7–6.6 ml·min^{-1}·kg^{-1}), and Pla (0.7–2.5 mmHg).

Table 3. *Hemodynamic data before, during, and after the closed-loop control of hemodynamics*

	Before (n = 12)	During (n = 12)	After (n = 11)
HR, beats/mm	147.4 (26.8)	149.4 (25.0)	135.7 (25.2)†‡
AP, mmHg	86.7 (22.4)	97.0 (7.4)	75.2 (21.1)‡
CO, ml·min^{-1}·kg^{-1}	53.7 (14.6)	96.7 (5.3)†	53.5 (8.6)‡
Pla, mmHg	21.8 (5.5)	10.8 (1.2)†	18.5 (3.4)‡
Pra, mmHg	6.9 (1.8)	4.4 (0.9)†	7.4 (2.2)‡
S_L, ml·min^{-1}·kg^{-1}	14.3 (4.0)	32.7 (2.6)†	15.1 (2.9)‡
R, mmHg·min·ml^{-1}·kg	1.5 (0.3)	1.0 (0.1)†	1.3 (0.4)*‡
V, ml/kg	34.2 (4.9)	28.5 (2.3)†	34.0 (5.4)‡

Values are means (SD). *$P < 0.05$, †$P < 0.01$ vs. Before; ‡$P < 0.01$ vs. During.

DISCUSSION

To the best of our knowledge, the automated drug delivery system we have developed is the first to successfully control AP, CO, and Pla simultaneously with reasonably good accuracy and stability. In a canine model of acute heart failure, our system automatically normalizes AP, CO, and Pla and maintains the levels stably within the desired ranges. Therefore, our system is potentially useful in the management of patients with acute decompensated heart failure.

Previous Closed-Loop Systems Controlling Hemodynamic Variables

Several previous systems have attempted to control two hemodynamic variables simultaneously (18, 26, 27). However, it is difficult to expand them to closed-loop control of the overall hemodynamics.

Voss et al. (26) and Yu et al. (27) reported closed-loop systems to control AP and CO using inotropes and vasodilators in dogs. In these systems, all possible input-output relations between drug infusion and the response of the controlled variable have to be estimated; namely, inotrope-AP, inotrope-CO, vasodilator-AP, and vasodilator-CO relations. The reason for this is that these drugs affect AP and CO simultaneously to almost the same degree. If this approach is applied to simultaneous control of AP, CO, and Pla, at least nine input-output relations have to be estimated, because at least three drugs are required to independently control the three variables. This would make the system extremely complicated and therefore be practically unfeasible.

In addition, the input-output relations must be estimated online in individual animals to tune the drug controllers. The reason for this is that the relations differ widely between animals and within animal over time. Even the direction of the

output response can change. For example, CO usually increases in response to SNP infusion in subjects with failing hearts but may also decrease in subjects with preserved cardiac function (23, 26). In the closed-loop system of Voss et al., such estimation induced unacceptably large fluctuations in AP (26). The feasibility of such online estimation is questionable when drug infusion rates are allowed to vary simultaneously because of the difficulty to differentiate between drug effects. To avoid this problem, Hoeksel et al. (18) allowed only one drug to be varied at a time, whereas other drugs were kept constant in closed-loop control of AP and pulmonary arterial pressure during cardiac surgery. However, their adjustments of volume supplementation or dobutamine infusion were manual. Their system did not completely automate the control of hemodynamics.

Characteristics of Our System

Our system controls the cardiovascular parameters characterizing the integrated CO curve, venous return surface, and arterial resistance and as a result achieves target values for hemodynamic variables. Compared with previous systems, our system may appear to adopt a rather roundabout approach. Our concept is that controlling the cardiovascular parameters is physiologically more rational, because it is equivalent to directly controlling the mechanical determinants of circulation. As indicated by Guyton et al. (16, 17), when the mechanics of the circulation are considered, the hemodynamic variables such as AP, CO, and atrial pressures are the effects, or dependent variables. Blood volume and the mechanical properties of the heart and vasculature, such as heart rate, ventricular contractility, and vascular resistance, are the causes, or independent variables. The integrated CO curve and venous return surface display these properties through the relationship between the flow and atrial pressures (24, 25). The total artificial heart control system developed by Abe et al. (1) adjusted its output in accordance with the vascular conductance (1/resistance) and AP, thereby achieving appropriate response to peripheral metabolic demands and avoiding hemodynamic abnormalities exhibited by other total artificial heart control systems. Their results also suggest that it is essential to consider the mechanical determinant of circulation for the control of the hemodynamic variables.

Our approach is advantageous from the perspective of control engineering. The three drug controllers (Fig. 2*A*) are designed on the basis of only four input-output relations between the drug infusion and the response of the controlled parameter; namely, Dob-S_L, SNP-R, Dex-V, and Fur-V (Fig. 3). We also found that Dob decreases R and increases V, and SNP increases S_L and decreases V (data not shown), which are compatible with previous studies (7, 22, 23). If these secondary effects induce significant interactions among the three closed loops, additional controllers would be needed to compensate for the interactions (4). However, our results indicate that these secondary effects are small enough to be compensated by the three drug controllers, and additional controllers are not necessary. The fact that the three closed loops are effectively decoupled drastically simplifies the entire system. This also permits system operators to understand its behavior easily (4).

Although we fix the PI gain constants and the constants of if-then rules, controls of cardiovascular parameters are accurate and stable (Fig. 4*B*). There are interindividual differences in the response of the parameters to drug infusion (Fig. 3). There should also be intraindividual differences in the response over time. However, our results indicate that the three drug controllers effectively compensate for all of these differences and do not require adaptive tuning in individual animals as in the previous system. As long as each cardiovascular parameter responds sensitively to the corresponding agent, our system is able to achieve target values for all the parameters, thereby achieving target hemodynamic variables.

Our system explicitly quantifies cardiac pump function, preload, and afterload, thereby controlling the overall hemodynamics. We believe that this unique feature of our system is intuitively appealing and is acceptable to clinicians.

Clinical Application of Our System

Our system will reduce the stress and work imposed on physicians and nurses who are managing patients with unstable hemodynamic conditions. These personnel will be able to spend more time on other patient-related activities, thereby improving the quality of patient care (10, 11). We believe that the closed-loop control of overall hemodynamics can extend the improvement in postoperative outcome demonstrated by Chitwood et al. (10) to various aspects of clinical cardiology or cardiac surgery.

In clinical settings, multisystem disorders such as renal disease, anemia, and diabetes may affect the performance of our system. Renal disease can weaken the response of V to the infusion of Fur. The hemodynamic changes in anemia include increased preload and reduced arterial resistance as compensatory mechanisms for the reduced oxygen-carrying capacity of the blood (8). These changes may affect the control of V and R by our system. In patients with diabetic cardiomyopathy, the sensitivity of S_L to Dob infusion may be reduced (5). Drugs prescribed before hospitalization such as β-blockers, or used during hospitalization such as morphine may also affect the performance of our system. Chronic β-adrenergic blockade can weaken the sensitivity of S_L to Dob infusion (2). Administration of morphine may change the response of V and R to the drugs infused (15). We must clarify these effects on the performance of our system as thoroughly as possible before our system can be considered for clinical application.

In the routine clinical environment, CO, and pulmonary artery occlusion pressure, a substitute for Pla, are measured intermittently with a Swan-Ganz catheter. For clinical application of our system, it is a prerequisite to monitor these variables continuously. Several methods have been developed to continuously monitor CO or the pulmonary artery occlusion pressure (6, 12). Integrating these methods into our system would bring the clinical application of our system closer to reality.

Limitations

All the experiments of this study were conducted in anesthetized, open-chest dogs. Anesthesia and surgical trauma affect the cardiovascular system significantly. Whether the present system is efficacious in conscious, closed-chest animals (including humans) remains to be seen.

We parameterized the integrated cardiac output curve and the venous return surface using *Eqs. A1*, *A2*, and *A4* (24, 25). Even if the actual curve or surface deviate slightly from those

estimated by these equations, our system compensates such deviations by the negative feedback mechanism. However, we did not confirm whether the estimation works well outside the physiological ranges of Pla and Pra, particularly under low atrial pressures (24, 25). The efficacy of our system in such conditions remains to be evaluated.

Our system controls R with vasodilators only and lacks a controller to increase R with vasoconstrictors. This will not be a major problem because the pathophysiology of acute heart failure is characterized by excessive vasoconstriction due to enhanced activity of sympathetic and renin-angiotensin systems (19). Vasoconstrictor control is necessary, however, for the management of patients with excessive vasodilatation, such as those in septic shock (21).

In this study, control of S_L was accurate and stable. However, it would be impossible to restore S_L pharmacologically if S_L is more severely depressed than those seen in this study as in the case of more diffuse myocardial disease or superimposed coronary artery disease. We must clarify in future studies to what magnitude of S_L depression can our system restore it reliably. In addition, how to use our system with mechanical circulatory support such as the intra-aortic balloon pump in case of the severe S_L depression remains to be established.

In the present design, if S_L is unable to respond to the infusion of Dob, the system will automatically increase the infusion rate of Dob owing to its negative feedback mechanism. This would be problematic especially in case of arrhythmia, which is a serious noise in the closed-loop control of S_L. If not appropriately suppressed, frequent premature ventricular contractions or ventricular tachycardia will depress S_L owing to disorganized ventricular contraction. In response to the depressed S_L, the system automatically increases the infusion rate of dobutamine. This could further exacerbate the arrhythmia, thus leading to a vicious cycle and collapse of the hemodynamics. To prevent such malfunction, a smart "sensor" that will filter these unwanted artifacts should be included in our system.

In the present study, we recorded only the urine volume. Measurement of urine flow and sodium excretion is essential to evaluate renal function, which is a very important prognostic indicator in patients with acute decompensated heart failure (14). It would be desirable to add the monitoring of these parameters to our system to improve the quality of patient care.

In conclusion, by directly controlling the mechanical determinants of circulation, our automated drug delivery system allows simultaneous control of AP, CO, and Pla with reasonable accuracy and stability and is potentially a powerful clinical tool for the management of patients with acute decompensated heart failure.

APPENDIX A

Parameters of Integrated Cardiac Output Curve, Venous Return Surface, and Arterial Resistance

We parameterized the integrated CO curve, the venous return surface and the systemic arterial resistance on the basis of previous studies (24, 25). In the integrated CO curve, CO ($ml \cdot min^{-1} \cdot kg^{-1}$) is closely related to Pla (mmHg) by the following formula (24):

$$CO = S_L \times [\ln(Pla - 2.03) + 0.80] \quad (A1)$$

and CO to Pra (mmHg) as follows:

$$CO = S_R \times [\ln(Pra - 1.0) + 0.88] \quad (A2)$$

S_L and S_R ($ml \cdot min^{-1} \cdot kg^{-1}$) are parameters representing the preload sensitivity of CO, i.e., the pumping ability of the left and right heart, respectively. These relations are consistent among different animals (24). In a preliminary study, we found that the ratio of S_R to S_L (α) remains fairly constant during infusion of dobutamine (data not shown). This suggests that once we know α, we can predict S_R in relation to a known change in S_L. Therefore we used S_L to parameterize the integrated CO curve. S_L can be calculated from CO and Pla by rewriting *Eq. A1* as follows:

$$S_L = CO/[\ln(Pla - 2.03) + 0.80] \quad (A3)$$

The venous return surface can be mathematically expressed by the following formula (25):

$$CO_V = V/0.129 - 19.61Pra - 3.49Pla \quad (A4)$$

V (ml/kg) is total stressed blood volume, and CO_V ($ml \cdot min^{-1} \cdot kg^{-1}$) is integrated venous return from systemic and pulmonary circulations. This relationship is also consistent among different animals (25). We used V to parameterize the venous return surface. V can be calculated from CO (= CO_V), Pla, and Pra by rewriting *Eq. A4* as follows:

$$V = (CO + 19.61Pra + 3.49Pla) \times 0.129 \quad (A5)$$

We parameterized the systemic arterial resistance (R) ($mmHg \cdot ml^{-1} \cdot min \cdot kg$) by the following formula:

$$R = (AP - Pra)/CO \quad (A6)$$

APPENDIX B

Determination of Target Parameters

On the basis of AP*, CO*, and Pla*, our system determines S_L*, V*, and R* as follows: S_L* is calculated by substituting CO* and Pla* into *Eq. A3*. By substituting baseline CO, Pla, and Pra into *Eqs. A1* and *A2*, baseline S_L and S_R are calculated to determine α. S_R (S_R*) corresponding to S_L* is predicted as:

$$S_R^* = \alpha \cdot S_L^* \quad (B1)$$

From *Eq. A2* and *B1*, target Pra (Pra*) is predicted as:

$$Pra^* = \exp[(CO^*)/(S_R^*) - 0.88] + 1.0 \quad (B2)$$

By substituting CO*, Pla*, and Pra* into *Eq. A5*, V* can be determined. By substituting AP*, CO*, and Pra* into *Eq. A6*, R* can be calculated.

GRANTS

This study was supported by Grant-in-Aid for Young Scientists (B) (16700379) from the Ministry of Education, Culture, Sports, Science and Technology, by Health and Labour Sciences Research Grants for Research on Medical Devices for Analyzing, Supporting and Substituting the Function of Human Body (H15-physi-001) from the Ministry of Health Labour and Welfare of Japan, and by the Program for Promotion of Fundamental Studies in Health Science of the National Institute of Biomedical Innovation. This study was also conducted as a part of "Ground-based Research Announcement for Space Utilization" promoted by Japan Space Forum.

REFERENCES

1. **Abe Y, Chinzei T, Mabuchi K, Snyder AJ, Isoyama T, Imanishi K, Yonezawa T, Matsuura H, Kouno A, Ono T, Atsumi K, Fujimasa I, and Imachi K.** Physiological control of a total artificial heart: conductance- and arterial pressure-based control. *J Appl Physiol* 84: 868–876, 1998.
2. **Antman EM, Anbe DT, Armstrong PW, Bates ER, Green LA, Hand M, Hochman JS, Krumholz HM, Kushner FG, Lamas GA, Mullany CJ, Ornato JP, Pearle DL, Sloan MA, and Smith SC Jr; American College of Cardiology; American Heart Association; Canadian Car-**